

Adsorption of Phenylboronic Acid Derivatives on Rutile TiO₂(110)

Published as part of *The Journal of Physical Chemistry C virtual special issue "Francesc Illas and Gianfranco Pacchioni Festschrift"*.

Alexander Wolfram, Maximilian Muth, Federico J. Williams, Sascha Mehl, Nataliya Tsud, Hans-Peter Steinrück, and Ole Lytken*



Cite This: <https://doi.org/10.1021/acs.jpcc.4c03264>



Read Online

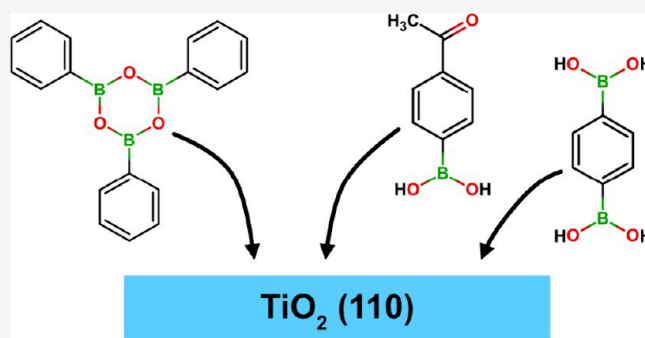
ACCESS |

Metrics & More

Article Recommendations

Supporting Information

ABSTRACT: Using high-resolution synchrotron-radiation photoelectron spectroscopy and near-edge X-ray-absorption fine structure, we have investigated the adsorption of three phenylboronic acid derivatives on rutile TiO₂(110) at 300–700 K: 4-acetylphenylboronic acid, 1,4-phenylenediboronic acid, and 2,4,6-triphenylboroxine. Both 4-acetylphenylboronic acid and 1,4-phenylenediboronic acid adsorb in a singly deprotonated monodentate configuration at 300 K, which converts to a fully deprotonated bidentate species at 550 K. 2,4,6-Triphenylboroxine undergoes a ring-opening reaction upon adsorption on the surface and forms the fully deprotonated bidentate species already at 300 K. In the case of 1,4-phenylenediboronic acid, the upward-pointing boronic-acid groups polymerize into boronic anhydride chains upon heating starting at 350 K. For 2,4,6-triphenylboroxine, we find a slow boron–carbon bond cleavage over a wide temperature range, resulting in a slow disappearance of the phenyl rings from the surface. For 4-acetylphenylboronic acid, we observe a loss of the carbonyl group at 500–550 K. In addition, we observe the formation of trigonal boron oxide (B₂O₃) for all three molecules at temperatures above 600 K.



INTRODUCTION

Boronic acids are Lewis acids, and the boron atom is prone to nucleophilic attacks. This is manifested, for instance, in the formation of the anion R-B(OH)₃[−] in aqueous solution by a nucleophilic attack of the oxygen atom of a water molecule, which subsequently loses a proton. In this reaction, the boron atom not only becomes negatively charged, but it also changes its local geometry from trigonal planar to tetrahedral. A nucleophilic attack on the boron atom by oxygen is also a reaction step in the well-known Suzuki coupling reaction,¹ in which the organic moiety of an organoboronic acid is coupled to the organic moiety of an organohalide. The Suzuki coupling reaction is an important synthetic reaction, as it is scalable and cost-effective, it allows for mild reaction conditions with relatively cheap reagents, and organoboronic acids are less toxic than the alternatives.^{2,3}

Boronic acids are also known to form bonds with diols through water elimination, creating new B–O–C bonds and water. This can be used for sensing or separating sugars by incorporating boronic acid groups into polymers or metal organic frameworks^{4–8} and allows boronic acids to be used as anchors for, e.g., glycoproteins or enzymes on organic layers⁹ in the same way that thiols can be used for gold surfaces^{10,11} and silanes for oxide surfaces.^{12,13} Less is known about the

interaction of boronic acids with metal oxide surfaces. The interactions of other groups, such as carboxylic acids, phosphonic acids, and silanes, with metal oxides have been studied more frequently, and applications such as electronics, solar cells, sensors, and anticorrosion coatings have been demonstrated;^{14–17} however, very few studies exist for organoboronic acids.^{14,18,19}

In this paper, we present a systematic study of three phenylboronic-acid derivatives, 4-acetylphenylboronic acid, 1,4-phenylenediboronic acid, and 2,4,6-triphenylboroxine, deposited on rutile TiO₂(110) under ultrahigh vacuum. Evaporation is the cleanest way to deposit molecules in a vacuum, but evaporating organoboronic acids comes with challenges: As mentioned above, boronic acids are reactive toward OH groups, including B–OH groups, making them extremely susceptible to anhydride formation and oligomeriza-

Received: May 22, 2024

Revised: July 2, 2024

Accepted: July 3, 2024

tion. This may be desirable, for example, when building two-dimensional networks,^{20–22} but it is a major problem when trying to evaporate the pure acid in a vacuum. We found that 4-acetylphenylboronic acid and 1,4-phenylenediboronic acid can be successfully evaporated under ultrahigh vacuum, without significant codeposition of the respective anhydride. Phenylboronic acid, however, decomposes slowly under evaporation conditions to 2,4,6-triphenylboroxine. We therefore decided to include 2,4,6-triphenylboroxine in our study to investigate the effect of intentional (or accidental) deposition of anhydrides during boronic acid deposition.

EXPERIMENTAL SECTION

A small number of reference measurements were carried out at our home lab in Erlangen, Germany, but unless stated otherwise, all measurements were performed at the Materials Science Beamline at Elettra-Sincrotrone in Trieste, Italy.

To minimize the anhydride formation during deposition, we used a home-built evaporator with a very large (16 cm²) graphite crucible, positioned as close as possible (3 cm) to the TiO₂(110) single-crystal surface. The molecules were sprinkled as a thin layer across the flat 16 cm² surface of the crucible. Compared to conventional evaporator setups, our specific setup lowered the evaporation temperatures by roughly 100 K, to 315, 350, and 310 K (± 5 K) for 4-acetylphenylboronic acid, 1,4-phenylenediboronic acid, and 2,4,6-triphenylboroxine, respectively, at deposition rates of about 0.05 ML/min. Channels inside the copper block holding the graphite crucible allowed us to heat and cool the crucible by passing hot or cold air through the copper block.

Due to the low evaporation temperatures of our compounds, we were unable to bake the load lock we used as a deposition chamber. However, to minimize the background pressure of water and any potential hydrocarbons (including anhydrides from the evaporator), the load lock was pumped by a cryopump (1500 L/s) during deposition, in addition to the regular turbomolecular pump (260 L/s). For the transfer between the load lock and the analysis chamber, which had a base pressure of 2×10^{-10} mbar, we had to pass through the preparation chamber, which was pumped by a turbomolecular pump (210 L/s) in addition to a second cryopump (1500 L/s).

Before depositing onto the rutile TiO₂(110) single crystal, we verified the cleanliness of the deposits by evaporating the molecules directly into a Balzers QMA 400 mass spectrometer in our home chamber in Erlangen (see Figure S1). As mentioned above, our first test molecule, phenylboronic acid, always decomposed at least partially into 2,4,6-triphenylboroxine, but both 4-acetylphenylboronic acid and 1,4-phenylenediboronic acid evaporated intact. As expected, 2,4,6-triphenylboroxine also evaporated intact. The same batch of the three molecules was then used for deposition at the Materials Science Beamline.

1,4-Phenylenediboronic acid and 2,4,6-triphenylboroxine were used as supplied. However, to avoid unwanted deposition of anhydrides, it was necessary to recrystallize 4-acetylphenylboronic acid in a mixture of isopropyl alcohol and deionized water in a ratio of 1:10 creating fine, needlelike crystals, as can be seen in Figure S2. We were unable to obtain fine needles for phenylboronic acid; however, if one could obtain them, evaporation of the intact acid might be possible.

Before each deposition, the 5 mm \times 10 mm \times 1 mm rutile TiO₂(110) crystal (CrysTec GmbH Kristalltechnologie) was

cleaned by several cycles of sputtering (30 min, Ar⁺, 1 kV, 2×10^{-6} mbar), and annealed at 800 K for 30 min, and the expected (1 \times 1) structure was confirmed by low-energy electron diffraction (LEED). The crystal was midrange blue after the experiments, indicating only moderate reduction. The temperature of the crystal was measured by a K-type thermocouple glued directly onto the side of the rutile single crystal with Ceramabond 552 ceramic glue (Kager GmbH, Germany). We know, from our vast experience, that this gives much more accurate temperature measurements than setups where the temperature of the crystal is measured indirectly, as, for instance, the temperature of the tantalum boat the crystal is mounted in.

Coverages are calculated using the C 1s and Ti 2p peak-area ratios assuming a smooth overlayer. Multilayers of 1,4-phenylenediboronic acid partially desorb and partially polymerize (see Figure 9, presented later in this work), and therefore do not form a reproducible monolayer. Because of the uncertainty of how 2,4,6-triphenylboroxine binds to the rutile TiO₂(110) surface, we also did not want to use this as our definition of one monolayer. Therefore, we used the C 1s:Ti 2p ratio of a saturated layer of 4-acetylphenylboronic acid at 300 K as our monolayer definition for all three molecules. If we compare with C 1s:Ti 2p ratios for other adsorbates on rutile TiO₂(110), for which we know the absolute coverage, such as phenylphosphonic acid²³ and Zn(II)-tetraphenylporphyrin,²⁴ we can estimate that our monolayer corresponds to approximately 12.1 carbon atoms per two titanium-row atoms, or 1.5 4-acetylphenylboronic acid molecules per two titanium-row atoms.

A SPECS PHOIBOS 150 hemispherical energy analyzer was used for both synchrotron-radiation photoelectron spectroscopy (SRPES) and near-edge X-ray-absorption fine structure (NEXAFS) measurements. The data were measured as a heating series from 300 to 700 K in 50 K steps, and the sample was allowed to cool down to room temperature between each annealing step before starting the measurements. Although we never found evidence of beam damage, we always used different spots on the sample for each temperature step. SRPES spectra are normalized to the photocurrent of a gold mesh within the beam to account for variations in photon flux over time. We aligned the O 1s core-level spectra to the rutile TiO₂(110) O 1s substrate peak position at 530.0 eV, but since the magnitude of this shift never exceeded 0.25 eV (usually only 0.1 eV within a heating series), we decided not to align the other core-level spectra.

The O 1s signal of the adsorbed molecule overlaps with the signal of the substrate (see Figure 6, presented later in this work). It is therefore crucial to have the highest possible surface sensitivity to minimize the relative intensity of the substrate peak, as well as having the highest possible binding-energy resolution, to better separate the adsorbate components from the substrate components. We achieved this by using a kinetic energy of 100 eV for the emitted photoelectrons and a 50/100 μ m monochromator slit setting in combination with the lowest-possible pass energy of 2 eV. All SRPES measurements were done at a light incidence angle of 50° and a photoelectron emission angle of 10° relative to the surface normal, which is the same sample geometry used for the B K-edge NEXAFS measurements.

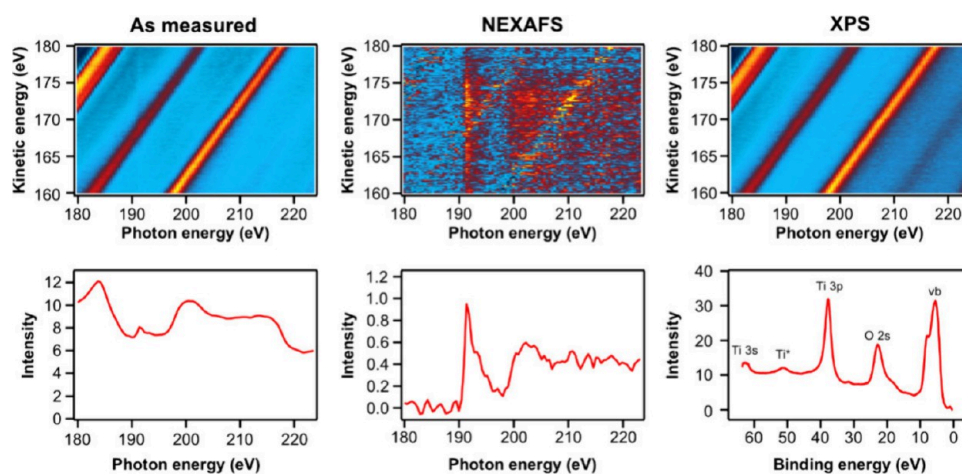


Figure 1. NEXAFS cleanup procedure²⁶ used to separate the vertical NEXAFS and diagonal XPS features in the as-measured Auger-yield NEXAFS spectral images. The example shown is the coarse-resolution B K-edge wide scan from Figure 2a of 0.3 ML 4-acetylphenylboronic acid on rutile TiO₂(110) after annealing at 450 K for 1 min, measured with polar and azimuthal E-field angles of 40° and 45°, respectively. The boron π^* resonance is only barely visible as a very faint vertical line at 190 eV in the as-measured image, but becomes clearly visible after cleanup, illustrating that this procedure enables access to systems previously inaccessible by Auger-yield NEXAFS. For visualization, a linear background is subtracted from the NEXAFS spectrum and from the NEXAFS image in the middle column.

METHODS

In NEXAFS, the 2-fold rotational symmetry of the rutile TiO₂(110) surface usually requires at least two different azimuthal crystal orientations to determine the polar and azimuthal orientation of adsorbed molecules. Unfortunately, the sample holder used at the Materials Science Beamline does not allow for azimuthal rotations inside the vacuum chamber, and removing the sample from the vacuum chamber to remount it would have been very time-consuming. We therefore chose to mount the sample at an electric-field azimuthal angle of 45°. Assuming that we are experimentally averaging over four mirror domains on the surface (see the Supporting Information), we become insensitive to the azimuthal orientation of the molecule on the surface at an electric-field azimuthal angle of 45°. This eliminates the need to remount the sample to determine the polar angle of the phenyl rings, saving a lot of time. We define an azimuthal orientation of 0° as being parallel to the oxygen rows, as determined by LEED. We also assume that the polarization of the incoming light is 0.8.²⁵

We wanted to measure B K-edge NEXAFS spectra at an electric-field polar angle of 50°, because, at this angle, the π^* intensity becomes independent of the molecular orientation, and thus any observed change is caused by a change in coverage or chemistry (see the Supporting Information for more details). Unfortunately, we measured instead at an electric-field polar angle of 40° (corresponding to a light incidence angle of 50°). This means that, although we expect chemical effects to dominate, we cannot exclude the possibility that changes in molecular orientation may cause some intensity variations.

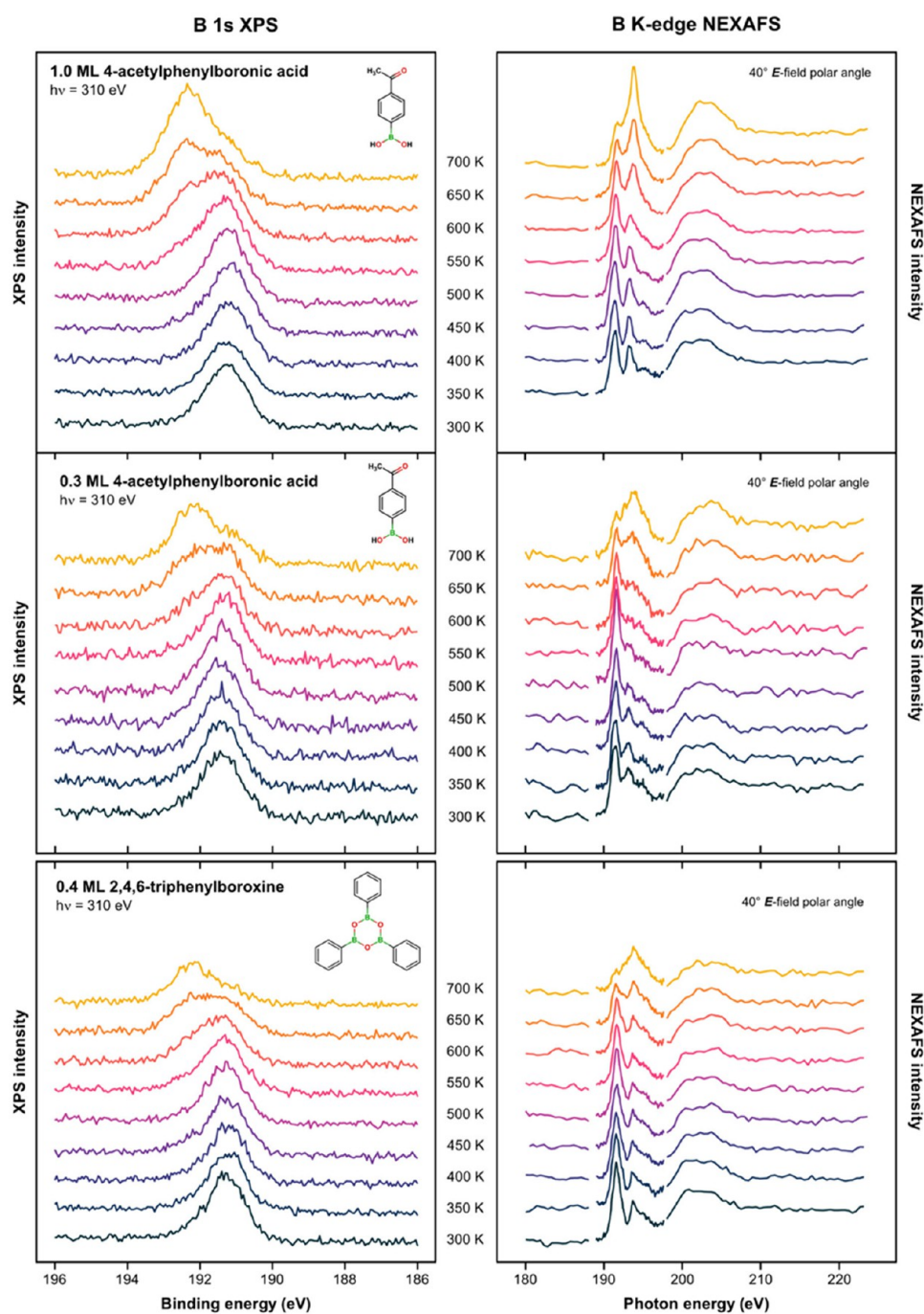
Auger-yield NEXAFS spectra suffer from XPS features traveling through the Auger regions, especially at monolayer and submonolayer coverage. This can be seen in Figure 1, where three intense diagonal XPS features (valence band, O 2s, and Ti 3p) dominate the faint vertical π^* resonance at 190 eV. We have developed a procedure that allows us to separate diagonal and vertical features and thus separate XPS and NEXAFS features.²⁶ The procedure is based on describing the

two-dimensional Auger-yield NEXAFS images as three one-dimensional spectra: XPS, Auger, and NEXAFS. An iterative algorithm is used to extract the three spectra, allowing us to remove the XPS contribution from the Auger image. After cleanup, the three main XPS features are still visible as three diagonal streaks of noise, but the improvement over the as-measured image is extreme, and both the π^* - and σ^* -NEXAFS features are clearly visible. The before and after spectra in Figure 1 clearly show how Auger-yield NEXAFS with this procedure can be used for systems that were previously inaccessible due to intense photoemission features.

After using the above procedure to remove photoemission features, we noticed a modest increase in background intensity in the B K-edge data at photon energies above 215 eV, where we would expect a flat plateau. The increase is also present for the clean TiO₂(110) surface and must therefore be related to a feature of the substrate, but we were not able to make a clear assignment. Nevertheless, we correct for this by subtracting the spectral image of the clean TiO₂(110) surface from the measured B K-edge images. Before subtraction, we scale the spectral image of the clean surface to the intensity of the Ti 3p peak traveling through the B K-edge images. After subtraction, we use the photoemission cleanup procedure to remove any remaining photoemission-feature remnants, caused by changes to the photoemission features between the clean rutile TiO₂(110) surface and the surface covered with molecules.

At the Materials Science Beamline, the optical elements are contaminated by carbon, leading to a significant (~70%) drop in photon flux at the C K-edge (see Figure S4). This can be corrected for by using the photocurrent of a clean gold mesh, but unfortunately, the gold mesh at the Materials Science beamline is also contaminated by carbon. Instead, we measure the photon flux for both the C K-edge and B K-edge as the intensity variation of the Au 4f peak of a freshly sputtered and annealed polycrystalline gold sample in the respective photon energy ranges (see Figure S4).

The large drop in photon flux at the C K-edge can also create second-order light artifacts,²³ because the drop in first-order light increases the relative intensity of the second-order light. Compared to a previous measurement, the artifacts were



(a)

Figure 2. continued

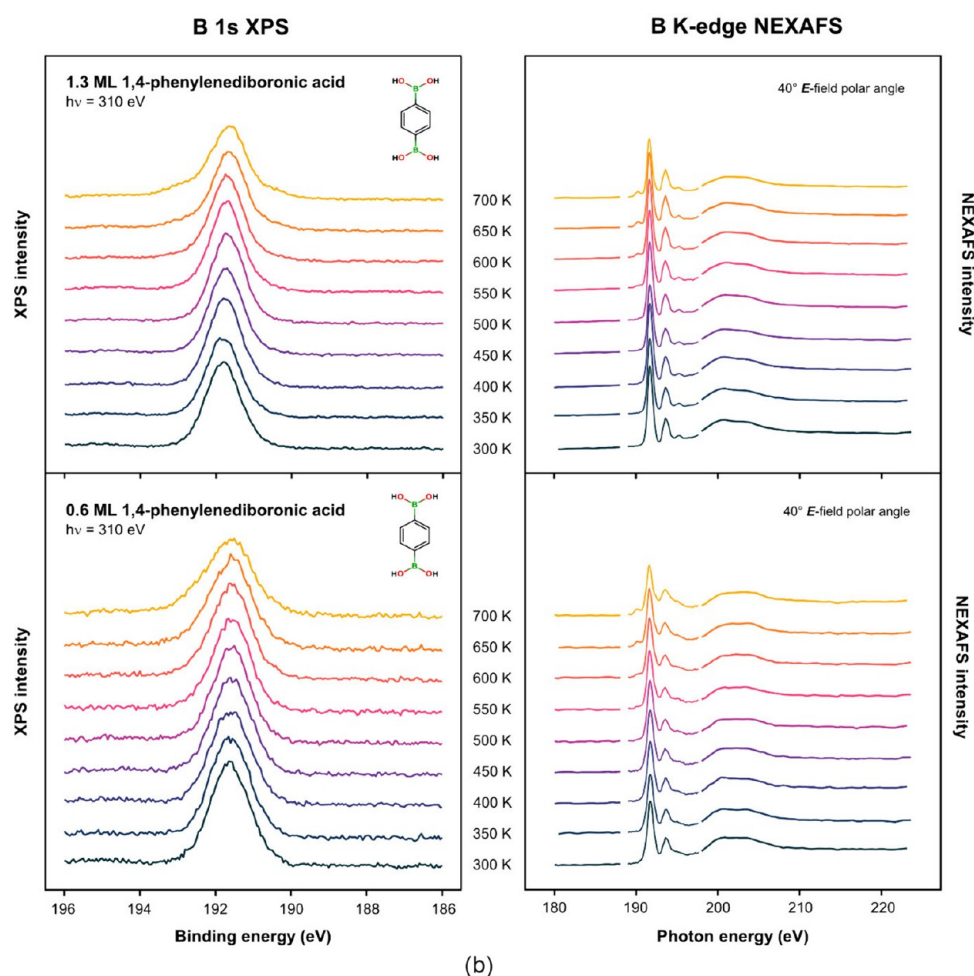


Figure 2. B 1s (left) and B K-edge NEXAFS (right) spectra of the three boronic acid derivatives ((a) 4-acetylphenylboronic acid and 2,4,6-triphenylboroxine and (b) 1,4-phenylenediboric acid) on rutile $\text{TiO}_2(110)$ after annealing at the indicated temperatures for 1 min. For visualization purposes, the XPS and NEXAFS spectra are normalized to the peak area and edge jump of the respective 300 K measurement. The breaks in the B K-edge NEXAFS spectra at 189 and 198 eV indicate the transition from the fine energy resolution we used for the π^* region to the coarse resolution we used everywhere else.

less pronounced, but we still corrected for them (for details, see the [Supporting Information](#) and ref 23).

RESULTS AND DISCUSSION

B 1s XPS and B K-Edge NEXAFS. Figure 2 shows the B 1s XPS and B K-edge NEXAFS spectra of the three boronic acid derivatives deposited on the rutile $\text{TiO}_2(110)$ surface at 300 K and annealed for 1 min at the indicated temperatures. It is immediately apparent from Figure 2a that the B 1s spectra of 4-acetylphenylboronic acid (top and middle) and 2,4,6-triphenylboroxine (bottom) are almost completely identical. They all show a single boron species at 191.3 eV, which is stable up to 500–550 K. Above 550 K, this species is gradually converted into a new boron species at 192.4 eV, and at 700 K the reaction is mostly complete. The same reaction is visible in the B K-edge NEXAFS spectra: Below 550 K, two to three π^* resonances with decreasing intensities are visible in all three heating series. Above 550 K, this is gradually converted to a single π^* resonance at 193.7 eV. The two to three resonances are consistent with what we would expect for the intact boronic acids (see the [Supporting Information](#)). This indicates that the observed signal originates from the intact molecules and not from impurities.

At first glance, the B 1s XPS and B K-edge NEXAFS spectra of 1,4-phenylenediboric acid appear different from those of the other two molecules (see Figure 2). However, when the B 1s spectra of 1,4-phenylenediboric acid are plotted on top of those of 4-acetylphenylboronic acid in Figure 3, the similarities become readily apparent: Although the 1,4-phenylenediboric acid spectra are dominated by a single B 1s peak, most likely from the unattenuated boronic acid group pointing away from the surface, the attenuated boronic acid group underneath, binding to the rutile $\text{TiO}_2(110)$ surface, behaves almost exactly like 4-acetylphenylboronic acid and thus also like 2,4,6-triphenylboroxine.

This means that all three molecules, independent of coverage, bind to the surface in an almost identical manner, and their bonds must be quite strong to be stable on rutile $\text{TiO}_2(110)$ up to 550 K, as shown in Figure 2. Keep in mind that we only need 310–350 K to evaporate the bulk powders. The coverage of the molecules on the rutile $\text{TiO}_2(110)$ surface, calculated based on the C 1s:Ti 2p ratios (see Figure S7), does suggest a slow gradual desorption (or loss of material) with increasing temperature, but nothing like a typical first-order desorption, which tends to be more abrupt.

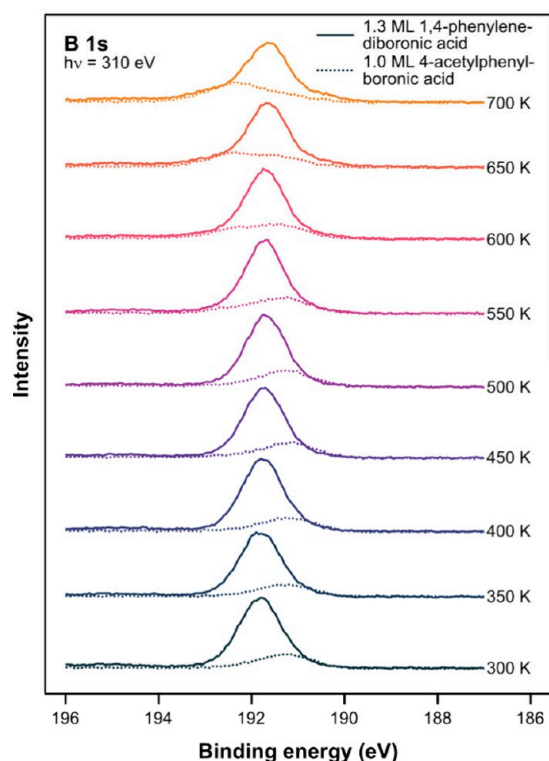


Figure 3. Comparison of the B 1s XPS spectra of 1.0 ML 4-acetylphenylboronic acid and 1.3 ML 1,4-phenylenediboronic acid on rutile $\text{TiO}_2(110)$ after annealing at the indicated temperatures for 1 min. The spectra of 1,4-phenylenediboronic acid are well-described by an unattenuated boronic acid group pointing away from the surface and a second, attenuated boronic acid group binding to the surface in the same manner as 4-acetylphenylboronic acid. The strong attenuation of the boronic acid group bonding to the surface of 1.3 ML 1,4-phenylenediboronic acid is consistent with the 85% attenuation we observe for the Ti 2p substrate signal.

The obvious candidates for a strong covalent bond are the boron and oxygen atoms of the boronic acid group. As mentioned in the **Introduction**, the boron atom of boronic acid is prone to nucleophilic attacks by oxygen, changing the trigonal planar coordination of boronic acid to a tetrahedral coordination. On the surface, the boron atom could react with an oxygen row atom and form a strong bond to the surface. This reaction would be clearly visible in B K-edge NEXAFS, where trigonal planar boron, such as in boric acid (crystalline^{27,28} or in water at pH 5²⁹) or in the mineral ludwigite ($\text{Mg}_2\text{Fe}^{3+}\text{BO}_3$),²⁷ is expected to have π^* - and σ^* -resonances at about 195 and 210 eV, respectively, whereas tetrahedrally coordinated boron, such as boric acid in water at pH 13²⁹ or in the mineral danburite ($\text{CaB}_2\text{Si}_2\text{O}_8$),²⁷ has only a broad σ^* -resonance, at 198 eV, and no π^* -resonances. For all temperatures and all coverages of all three molecules, we observe strong B K-edge π^* -resonances, and we can therefore exclude tetrahedrally coordinated boron as the primary adsorbed species on the surface, indicating that the boron atom is not bound to the surface and that the oxygen atoms of the boronic acid group are the most-likely site of a strong bond.

Possible On-Surface Species. Brønsted acids, such as carboxylic^{30,31} and phosphonic^{23,32,33} acids, are known to fully or partially deprotonate on rutile $\text{TiO}_2(110)$ and bind through the deprotonated oxygen atoms to the titanium atoms of the

exposed titanium rows on rutile $\text{TiO}_2(110)$. Even weak Brønsted acids, such as catechol,³⁴ bind in this manner. When comparing the C 1s:Ti 2p ratio of the saturated monolayer of 4-acetylphenylboronic acid on $\text{TiO}_2(110)$ with previously measured C 1s:Ti 2p ratios for monolayers of phenylphosphonic acid²³ and Zn(II)-tetraphenylporphyrin²⁴ (see the **Experimental Section**), we find that the saturation coverage of 4-acetylphenylboronic acid corresponds to 1.5 boronic acid molecules per two titanium-row atoms. This packing density strongly suggests that most of the boronic acid molecules in the saturated monolayer must be oriented perpendicular to the titanium rows of the substrate, with only one oxygen atom sitting on a titanium-row atom.

Density functional theory (DFT) calculations by O'Rourke et al.³⁵ of boronic acid ($\text{HB}(\text{OH})_2$) on rutile $\text{TiO}_2(110)$ find two stable adsorption geometries for isolated molecules: A fully deprotonated bidentate species adsorbed along the titanium rows, and a singly deprotonated monodentate species adsorbed perpendicular to the titanium rows. The bidentate species was found to be more stable, but only by 0.12 eV. The maximum-possible coverage for the bidentate species is one molecule per two titanium-row atoms, which is below our observed saturation coverage for 4-acetylphenylboronic acid of 1.5 molecules per two titanium-row atoms. However, it is not unreasonable for the monodentate species, which has the smaller surface footprint, to become increasingly favored as coverage increases. Our saturation coverage therefore strongly suggests that the species on the surface are either purely monodentate, or a 2:1 mixture of mono- and bidentate.

In the DFT calculations by O'Rourke et al.,³⁵ the B–OH group of the monodentate forms a hydrogen bond to an oxygen-row atom in the surface. At our observed saturation coverage of 1.5 molecules per two titanium-row atoms, most of the oxygen-row atoms are hydrogenated. However, by slightly rotating the boronic-acid group and placing the oxygen atom of the B–OH group between two surface Ti–OH groups, a zigzag-style hydrogen bonding between the B–OH and Ti–OH groups should be possible. We therefore think that the monodentate adsorption structure from O'Rourke et al.³⁵ is plausible, although the hydrogen bonding situation must be different from their calculation.

Regardless of the binding motif, in both monodentate and bidentate adsorption modes, the adsorbed molecule is partially or fully deprotonated and Ti–OH groups are formed on the surface. Experimentally, surface Ti–OH groups on rutile $\text{TiO}_2(110)$ are usually visible in the valence band as a peak at about 11 eV.^{36,37} In our data in **Figure S8a**, this feature is best visible in the valence-band spectra of 0.3 ML 4-acetylphenylboronic acid as a feature at 10.5 eV, which disappears above 500 K, consistent with the protons desorbing as water. For 1,4-phenylenediboronic acid in **Figure S8b**, the Ti–OH feature is not clearly visible, but this could be caused by the strong attenuation of the 33 eV photoelectrons passing through the molecular layer. For comparison, at a coverage of 1.0 ML the Ti 2p signal of our $\text{TiO}_2(110)$ substrate is attenuated by 75% at a kinetic energy of 100 eV.

For 0.4 ML 2,4,6-triphenylboroxine, we would not expect to see the Ti–OH feature at 10.5 eV, and, although we do see changes above 550 K close to this energy in **Figure S8a**, the changes are smaller and seem to be mostly related to the feature at 13.3 eV also observed in the 0.6 ML 1,4-phenylenediboronic acid spectra. As protons desorb from rutile $\text{TiO}_2(110)$ at 450–500 K as water, oxygen vacancies are

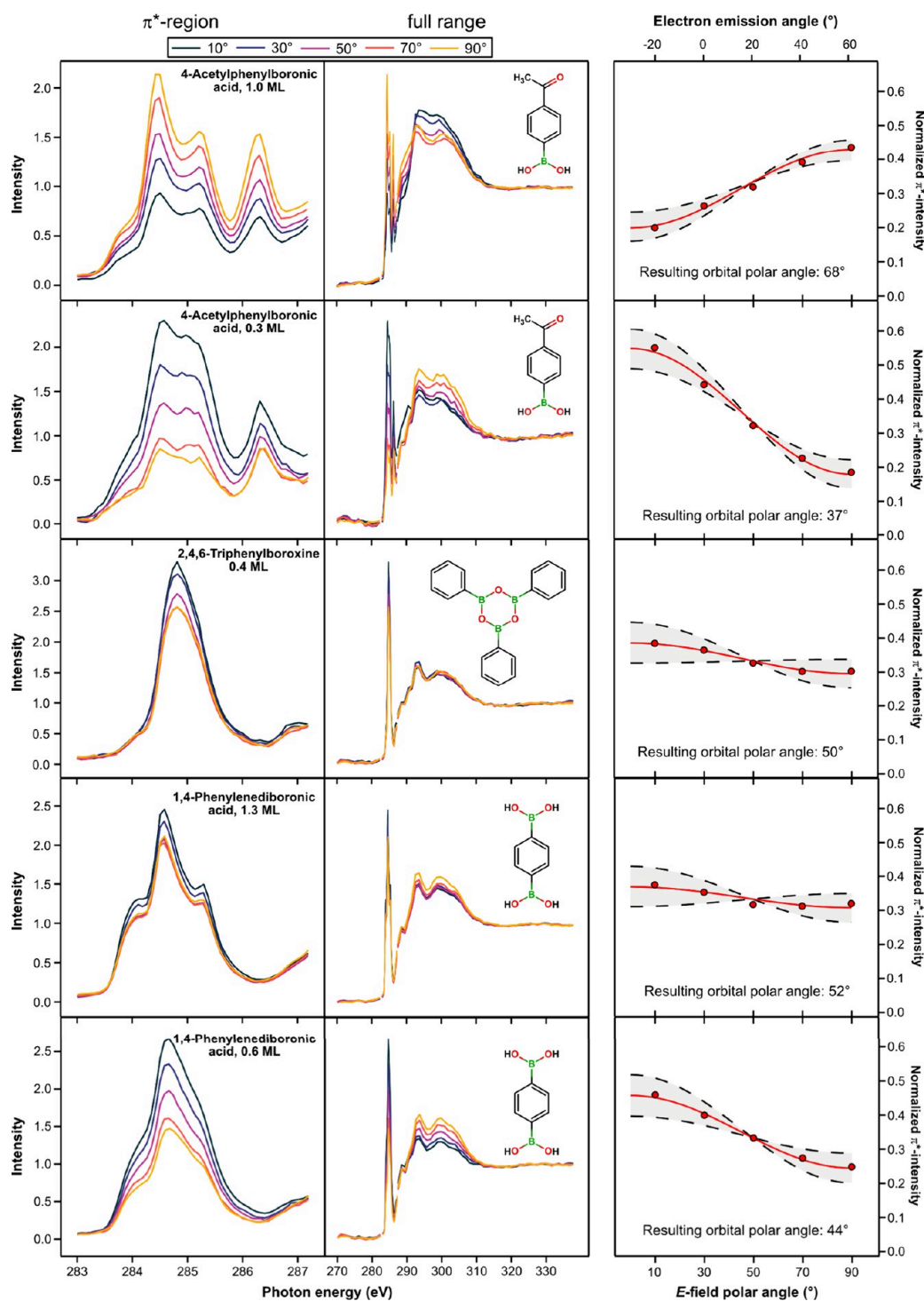


Figure 4. Angular-dependent C K-edge NEXAFS spectra for an E-field azimuthal angle of 45° of the three boronic acid derivatives on rutile $\text{TiO}_2(110)$ after annealing at 400 K for 1 min. The full NEXAFS spectrum (middle) has breaks at 283 and 287 eV, indicating the transition from the fine energy resolution we used for the π^* -region to the coarse resolution we used everywhere else. The area of the fine resolution π^* -peaks (left) changes as a function of the E-field polar angle and this change was used to extract the orbital polar angle relative to the surface normal (right). The red line indicates the best fit to a 2-fold symmetric substrate with four mirror domains assuming a polarization of 0.8,²⁵ and the dashed black lines indicate the calculated angular dependency if the orbital polar angle would vary by $\pm 5^\circ$.

formed in the oxygen rows.^{38,39} When this happens, we expect the remaining B–OH groups of the molecule to deprotonate and fill the vacancies, converting the low-temperature singly deprotonated monodentate into a high-temperature fully deprotonated bidentate species. This behavior is similar to that previously observed for phenylphosphonic acid²³ and

formic acid^{31,40} on rutile $\text{TiO}_2(110)$, and such a reaction has been considered in DFT calculations by Raghunath and Lin on boric acid ($\text{B}(\text{OH})_3$) on rutile $\text{TiO}_2(110)$.⁴¹ The boronic acid group has two protons, and therefore one oxygen vacancy is created per adsorbed molecule. This allows for different possible molecular orientations: If the oxygen vacancies are

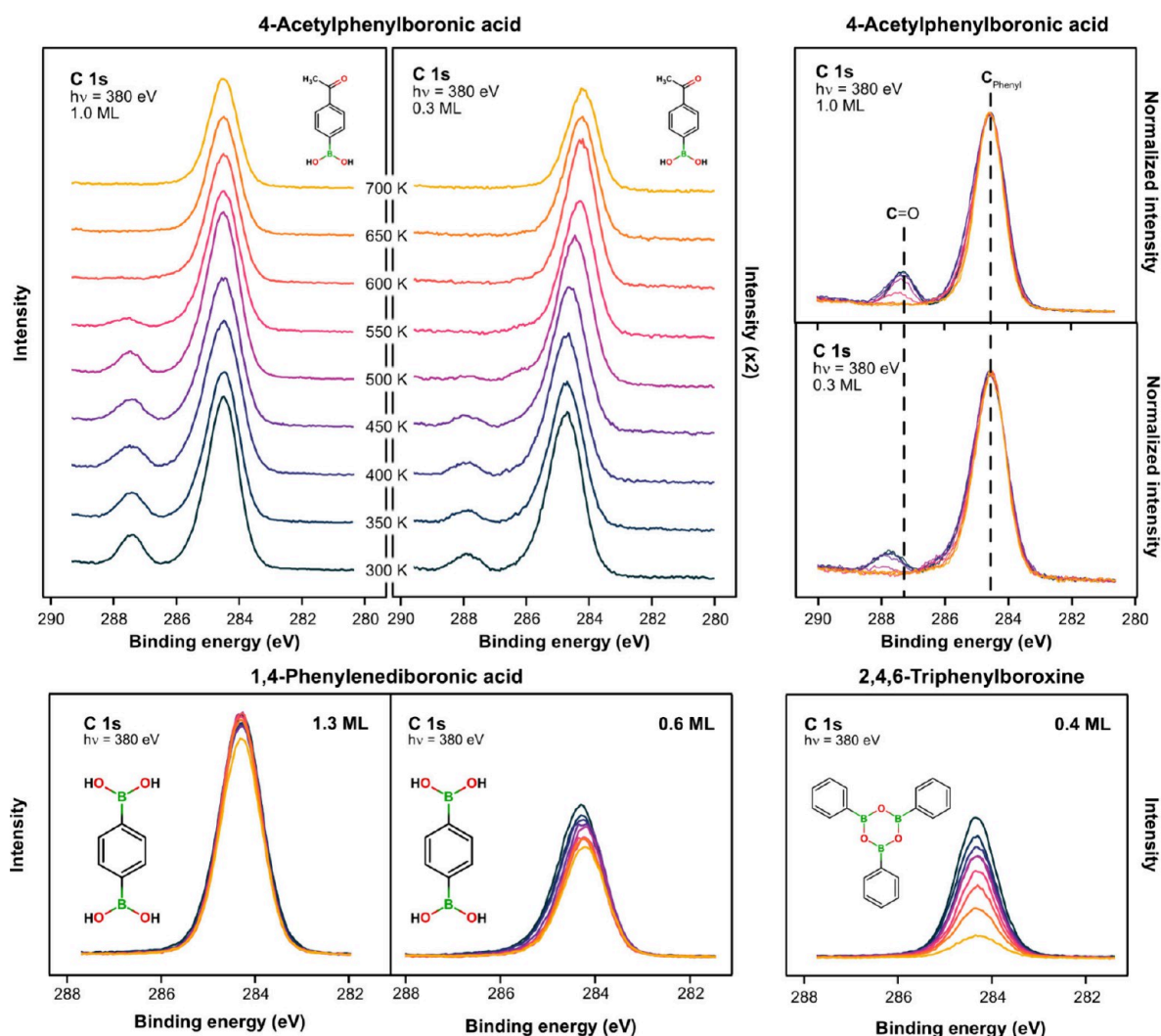


Figure 5. C 1s spectra of the three boronic acid derivatives on rutile $\text{TiO}_2(110)$ after annealing at the indicated temperatures for 1 min. 4-acetylphenylboronic acid is shown both as measured (top left), and normalized and aligned to the phenyl ring C 1s component (top right), to better show the changes in the carbonyl (C = O) group. 1,4-phenylenediboric acid (bottom left) and 2,4,6-triphenylboroxine (bottom right) are both shown as measured. The color scheme of all graphs corresponds to the same temperatures as indicated in the top left graph.

distributed evenly, with each adsorbed molecule adjacent to one vacancy, the boronic acid group would most-likely be oriented perpendicular to the titanium rows with one leg on a titanium row and one leg in the oxygen vacancy of the oxygen row. If instead the oxygen vacancies are unevenly distributed, with the adsorbed molecules alternating between being adjacent to two vacancies and no vacancies, the boronic acid groups would most likely alternate between both legs on the titanium rows, binding to no vacancies, and both legs in the oxygen rows filling two vacancies. In this scenario, all molecules would be parallel to the titanium rows. A mixture of the two scenarios would also be possible, alternating between perpendicular and parallel adsorption modes, creating a T-stacked structure. In this structure, the molecules parallel to the oxygen rows would alternate between both legs on the titanium rows and both legs in the oxygen rows.

If the low-temperature adsorption structure is purely monodentate, a coverage of 1.5 molecules per two titanium-row atoms would mean that every fourth titanium-row atom is left empty, and the average phenyl ring distance is 3.9 Å. This value is larger than the interlayer distance of graphene layers in graphite of 3.4 Å,⁴² and also the π - π stacking distance found

in the crystal structure of 2,4,6-triphenylboroxine of 3.4 Å^{43,44} or the phenyl ring distance in PTCDA of 3.7 Å.^{45,46} The π - π stacking distance required to form a pure monodentate structure with a saturation coverage of 1.5 molecules per two titanium-row atoms is therefore quite reasonable compared to other π - π stacked systems. However, T-type stacking is also possible, both at low temperature, if we have a 2:1 mixture between mono- and bidentate, and at high temperature, if we have alternating perpendicular and parallel adsorption modes, as mentioned above. However, T-stacked systems usually have larger phenyl-ring spacing. In solid benzene, for instance, the distance is 4.7 Å,⁴⁷ which is significantly larger than the average phenyl-ring distance of 3.9 Å in our saturated layer. Assuming a typical π - π stacking distance of 3.5 Å and a typical T-type stacking distance of 4.7 Å, we can estimate the expected average stacking distance in a 2:1 mixed mono- and bidentate structure to be 4.3 Å. This is still slightly larger than the average phenyl-ring distance in our saturated layer of 4.0 Å. The average phenyl-ring distance in our saturated layer therefore strongly suggests a predominantly π - π stacked structure.

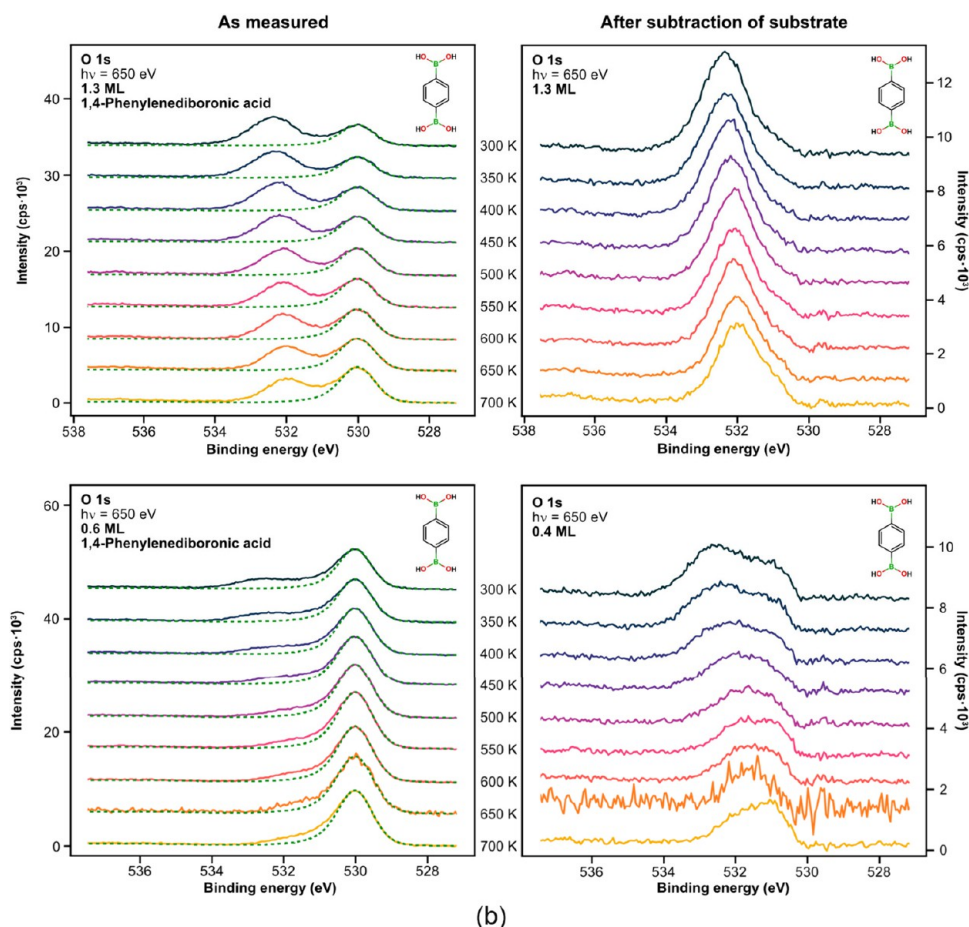


Figure 6. O 1s spectra of the three boronic acid derivatives ((a) 4-acetylphenylboronic acid and 2,4,6-triphenylboroxine and (b) 1,4-phenylenediboronic acid) on rutile TiO₂(110) after annealing at the indicated temperatures for 1 min. The O 1s spectra after subtraction of the substrate contribution (right) are obtained from the as-measured O 1s spectra (left), where the substrate contribution with the shape of the clean surface O 1s spectrum is indicated by a dashed green line. Slight changes in the substrate peak shape and position will cause artifacts at 530–529 eV after substrate subtraction, which is best visible for 0.3 ML 4-acetylphenylboronic acid at 700 K. All spectra are aligned to the substrate contribution at 530.00 eV.

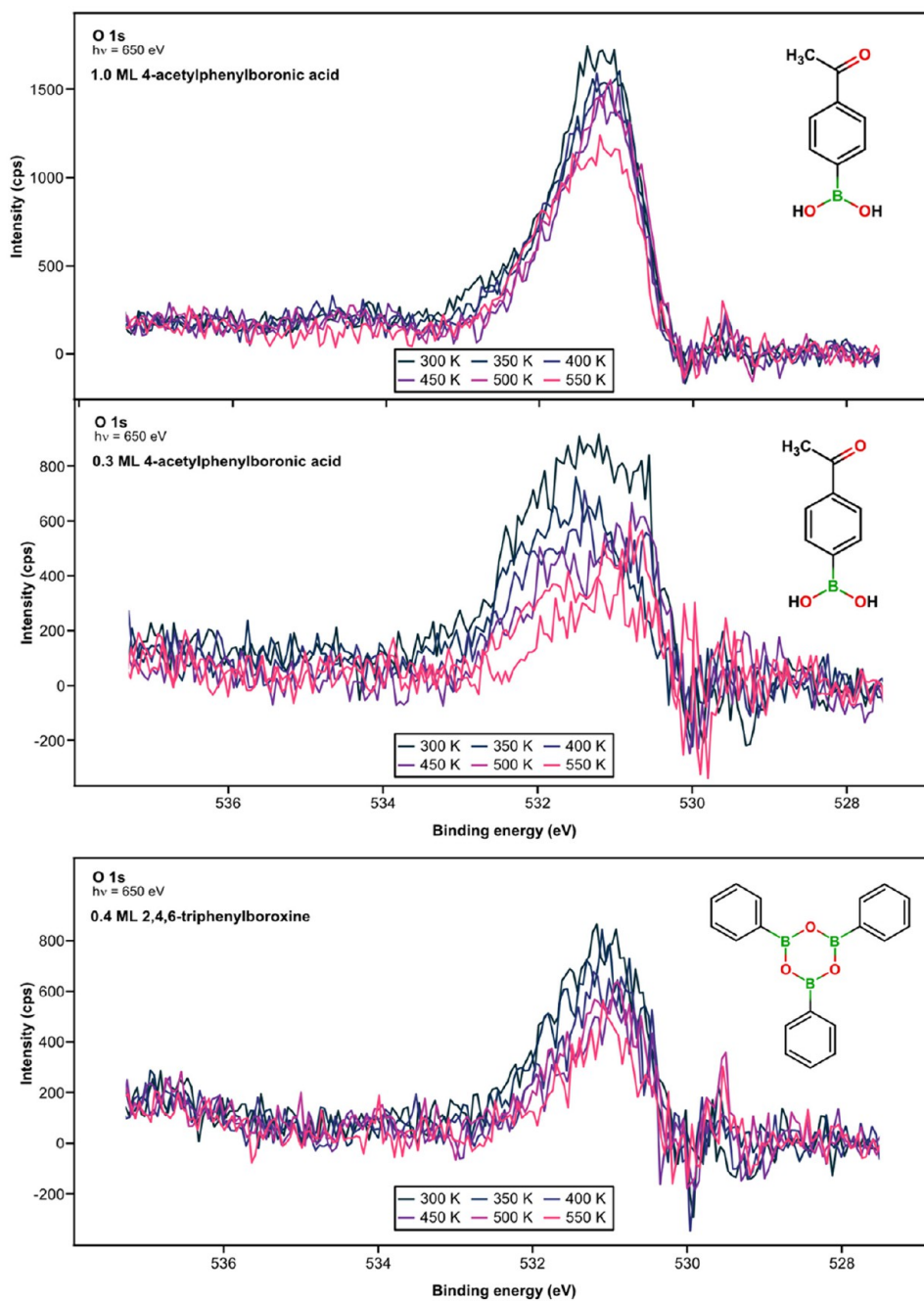
C K-Edge NEXAFS. Figure 4 shows the angular-dependent C K-edge NEXAFS spectra of the three molecules deposited on rutile TiO₂(110). It is immediately clear that the π^* regions look very different for the three molecules. However, this is consistent with our TD-DFT-predicted NEXAFS spectra of the gas-phase molecules in Figure S6. The larger number of π^* resonances at the C K-edge compared to the B K-edge is caused by the slightly different C 1s binding energies of the nonequivalent carbon atoms of the molecule. Because the width of peaks in XPS (see Figure 5) is wider than the width of π^* peaks in NEXAFS (see Figure 4), the effect of the nonequivalent carbon atoms becomes more pronounced in the NEXAFS spectra. The number of resonances we observe at the C K-edge is therefore consistent with what is expected for these molecules and is not a result of impurities.

As mentioned in the Experimental Section, we can use the angular dependency of the π^* resonances in C K-edge NEXAFS to calculate the polar angle, relative to the surface normal, of the orbital transition vector of the extended planar system consisting of the boronic acid group, the phenyl ring and the carbonyl group. This is done assuming a polarization of 0.8²⁵ and four mirror domains on the surface (see the Supporting Information for more details).

It is clear from Figure 4 that all the individual π^* resonances scale the same, consistent with all the relevant unoccupied states lying in the same plane, as expected for an extended planar system. This would not be the case if the boronic acid group, the phenyl ring and the carbonyl group were rotated relative to each other. Thus, we can use the integrated intensity of all the π^* resonances to calculate the polar angle of the molecules; the corresponding results are shown in Figure 4.

For 1.0 ML of 4-acetylphenylboronic acid at 400 K, this yields a polar angle of 68° between the orbital transition vector of the extended planar system and the surface normal, which is equal to the polar angle between the phenyl-ring plane and the surface plane. An angle of 90° thus corresponds to an upright-standing molecule, and 0° to a flat-lying one. In the following, we will refer to this angle as the adsorption angle of the molecule. At a coverage of 0.3 ML, the adsorption angle of 4-acetylphenylboronic acid decreases to 37°. This behavior is often observed in π - π stacked systems where molecules tilt down more and more in an attempt to keep the optimal distance between the phenyl rings.^{48,49}

For 1,4-phenylenediboronic acid, this behavior in Figure 4 is less pronounced, with the adsorption angle decreasing from 52° to 44° as the coverage decreases from 1.3 to 0.6 ML; this is



(a)

Figure 7. continued

O 1s core level after subtraction of substrate contribution

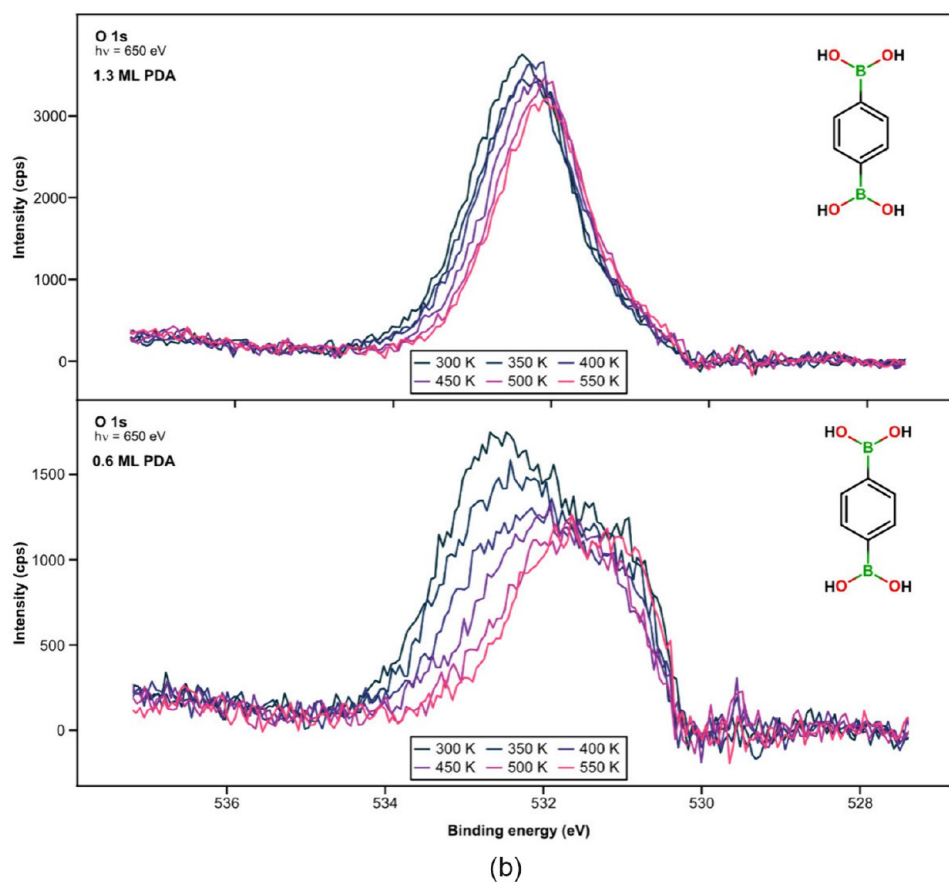


Figure 7. O 1s core-level spectra after substrate subtraction for (a) 4-acetylphenylboronic acid and 2,4,6-triphenylboroxine and (b) 1,4-phenylenediboronic acid. The spectra are the same as depicted in Figure 6, but here only the 300–550 K temperature range is shown, and the spectra within each series are plotted on top of each other to better visualize the trends.

most likely caused by flatter-lying multilayer molecules decreasing the apparent adsorption angle at 1.3 ML.

2,4,6-Triphenylboroxine bucks this trend, with an adsorption angle of 50° at 0.4 ML, which is more upright standing than the other two molecules at similar coverage. To explain why, we first need to understand how 2,4,6-triphenylboroxine binds to rutile $\text{TiO}_2(110)$.

The B 1s XPS and B K-edge NEXAFS spectra in Figure 2a strongly suggest that 2,4,6-triphenylboroxine forms a very similar species compared to the other two boronic acid derivatives on the surface. However, the intact 2,4,6-triphenylboroxine molecule cannot bind to the surface in the same manner as the other two boronic acid derivatives, unless the boroxine ring undergoes a ring-opening reaction. This could explain the low saturation coverage of 0.42 ML for 2,4,6-triphenylboroxine, as a ring-opening reaction would likely require a larger ensemble of adjacent sites. Because 2,4,6-triphenylboroxine and phenylboronic acid have the same appearance in the DFT-calculated B K-edge NEXAFS spectra in Figure S6, there will be no telltale signs in B K-edge NEXAFS that a ring opening reaction has taken place. It is important to remember that the only difference between 2,4,6-triphenylboroxine and phenylboronic acid is one water molecule per monomer, and that, as discussed above, surface Ti–OH groups on rutile $\text{TiO}_2(110)$ desorb as water above 450 K.^{38,39,50,51} Assuming chemical equilibrium is reached, the

adsorbed species formed by boroxine on $\text{TiO}_2(110)$ should therefore be identical to the species formed by adsorbing phenylboronic acid and heating above 450 K to desorb water. Consequently, we expect the species formed on rutile $\text{TiO}_2(110)$ upon adsorption of 2,4,6-triphenylboroxine at 300 K to be a bidentate species, oriented either perpendicular to the titanium rows with one leg on a titanium row and one leg in an oxygen row, or parallel to the titanium rows alternating between two legs on the titanium row and two legs in the oxygen row, or a mixture of the two.

The slightly more upright-standing adsorption angle of 2,4,6-triphenylboroxine in C K-edge NEXAFS at 400 K, compared to the other two boronic acid derivatives at comparable coverages in Figure 4, therefore suggests that the adsorption angle of the fully deprotonated bidentate species is slightly more upright standing than for the singly deprotonated bidentate.

O 1s XPS. A lot of information about the adsorbed species is found in the O 1s core-level region, but accessing this information is far from easy, due to the strong overlap of the adsorbate and substrate signals in Figure 6. It is therefore extremely important to have the best-possible surface sensitivity, which we achieve by using a kinetic energy of the emitted photoelectrons of about 100 eV, and the best-possible energy resolution, which we achieve by a combination of a low

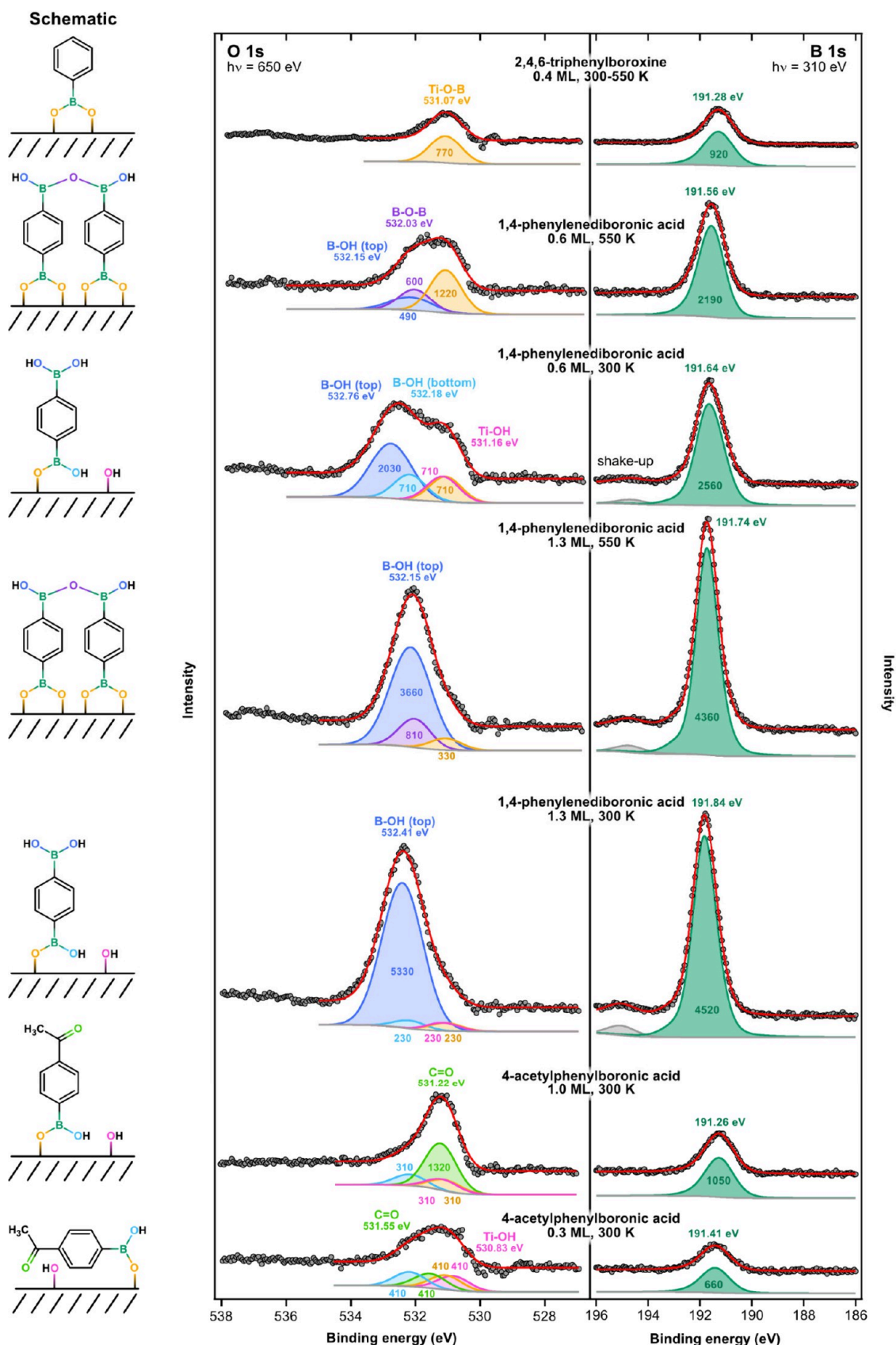


Figure 8. Selected substrate-subtracted O 1s and B 1s spectra from Figures 2 and 6 of the three phenylboronic acid derivatives deposited on rutile TiO₂(110) and annealed at the indicated temperatures for 1 min. The temperatures indicate plateaus where we believe stable species are formed. The stable species are shown schematically in the left column, and the colors for the various atoms correspond to the colors of the fitted peaks in the O 1s spectra.

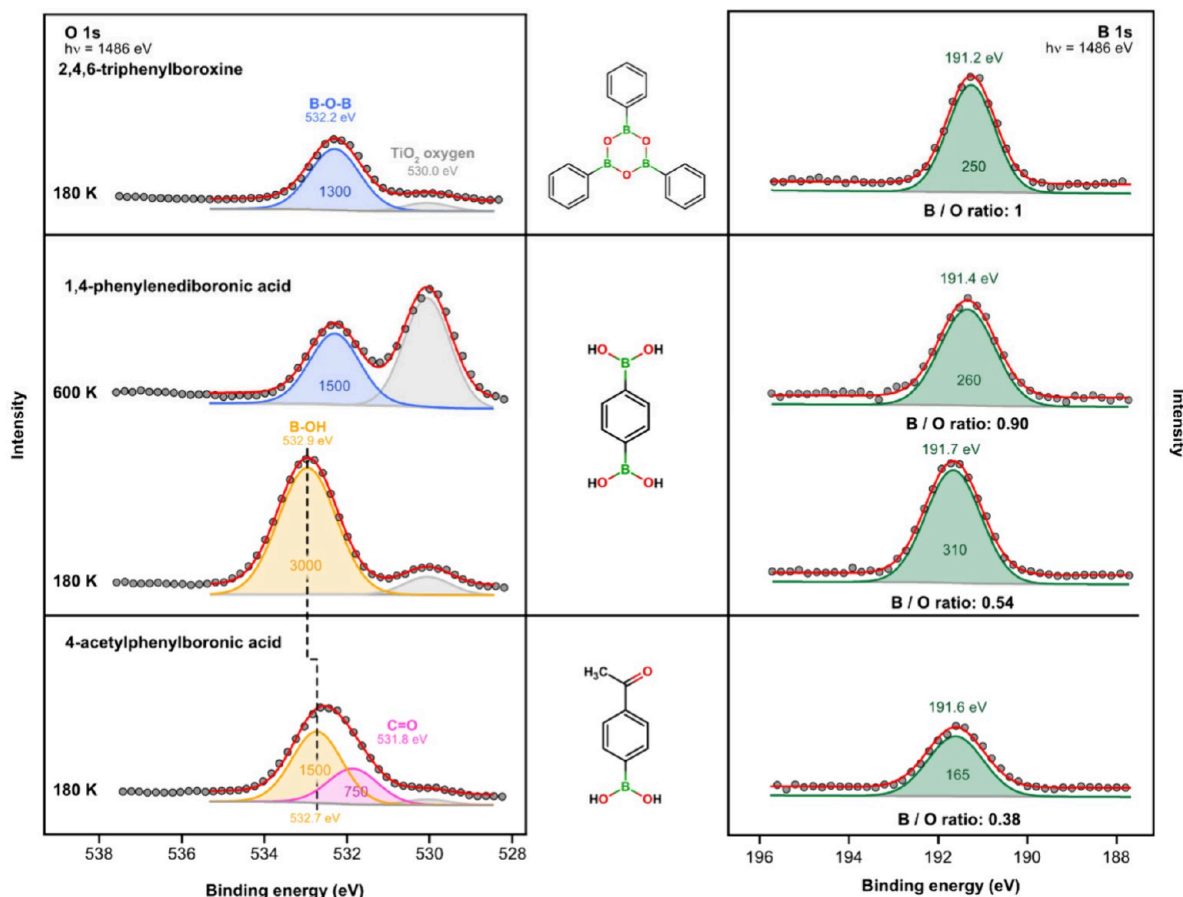


Figure 9. Laboratory source Al $K\alpha$ O 1s and B 1s spectra of multilayers of 1,4-phenylenediboronic acid, 2,4,6-triphenylboroxine, and 4-acetylphenylboronic acid deposited on rutile $\text{TiO}_2(110)$ at 180 K to avoid coadsorption of water. When annealing multilayers of 1,4-phenylenediboronic acid at 600 K for 1 min, we observe roughly half the molecules desorbing and the other half polymerizing. This is also reflected in the B:O ratio, which changes from 0.54 (expected for the intact molecule) to 0.90 (close to full polymerization). The B:O ratio is normalized to the B:O ratio of 2,4,6-triphenylboroxine, which is assumed to be 1. Spectra are aligned to the substrate oxygen position at 530.0 eV.

pass energy (2 eV) in the analyzer and narrow slits (50/100 μm) for the photon beam.

An additional problem is that the O 1s signal from the TiO_2 substrate is broadened significantly by a strong surface relaxation,²³ which can be lifted upon adsorption of molecules such as formic acid^{52,53} and phenylphosphonic acid.²³ This can narrow the O 1s peak of the substrate by up to 0.2 eV, making it difficult to subtract the substrate contribution from the measured O 1s spectra.²³ Fortunately, we only observe a modest (<0.1 eV) narrowing of the substrate O 1s peak upon adsorption of the three boronic acid derivatives. This allows us to fit and subtract the substrate contribution to the O 1s spectra reasonably well using the full shape of the clean-surface O 1s spectrum, while allowing for only a modest (<0.1 eV) change in peak width.

Figure 6 shows the O 1s spectra for the three boronic acid derivatives after deposition on rutile $\text{TiO}_2(110)$ at 300 K. The left column shows the as-measured spectra with the fitted substrate peaks marked by dashed green lines, and the right column shows the adsorbate-related O 1s components remaining after subtraction of the substrate peak.

For all three molecules, we will focus on the O 1s and also the B 1s spectra in the 300–550 K temperature range to begin with (see Figure 7). This is below the temperature where the oxidized B 1s species at 192.4 eV begin to appear (see Figure 2).

2,4,6-Triphenylboroxine. As discussed above, we expect the 2,4,6-triphenylboroxine molecule to undergo a ring-opening reaction on the surface, resulting in the formation of a fully deprotonated bidentate phenylboronic acid-like species. When we look at the O 1s and B 1s spectra of 0.4 ML 2,4,6-triphenylboroxine in the 300–550 K temperature range in Figure 7a and Figure 2a, we do indeed observe a single O 1s feature at 531.07 eV, consistent with the formation of two equivalent Ti–O–B bonds, and a single B 1s feature at 191.1 eV.

The B 1s peak area in Figure 2a is constant between 300 and 550 K, but the O 1s peak area in Figure 7a appears to decrease slightly. However, this slight apparent decrease could be caused by very small changes in the shape of the substrate peak (see Figure 6a), and we are therefore hesitant to consider this decrease to be significant. The decrease in the C 1s peak area in Figure 5, however, is very significant. This change could be caused by cleaving the carbon–boron bond, which boronic acids are prone to do.⁵⁴ We can only guess on the mechanism, but it could be a protolytic deboronation, where a hydrogen atom, presumably provided by surface hydroxyl groups, replaces the phenyl ring at the boronic acid group and the phenyl ring desorbs as benzene. The other two boronic acid derivatives also exhibit a small loss of carbon upon heating, as can be seen in Figure 5, but nowhere near as significant as 2,4,6-triphenylboroxine.

In conclusion, 2,4,6-triphenylboroxine undergoes a ring-opening reaction upon adsorption on rutile $\text{TiO}_2(110)$ already at 300 K, forming a fully deprotonated bidentate-bonded species (see Figure 8). Upon heating, a slow and steady loss of carbon is observed, but the bond to the surface through the boronic acid group remains unchanged.

0.6 ML 1,4-Phenylenediboronic Acid. The O 1s spectra of 0.6 ML 1,4-phenylenediboronic acid in the 300–550 K temperature range in Figure 7 show a low binding energy component at about 531 eV, which remains mostly unchanged upon heating, and a high binding energy component at about 533 eV, which decreases with increasing temperature and shifts to lower binding energies until a stable plateau is reached at 500–550 K. Interestingly, in the same temperature range the B 1s spectrum remains completely constant (see Figure 2). The decreasing oxygen-to-boron ratio in Figure 8, and the shift to lower O 1s binding energies is consistent with the anhydride formation, which we observe when desorbing multilayers of 1,4-phenylenediboronic acid (see Figure 9). Assuming no polymerization at 300 K, we can estimate the degree of polymerization at 550 K based on the decreasing oxygen-to-boron ratio from Figure 8 (see the Supporting Information for more details). This approach yields a polymerization degree of 71%, meaning that 71% of the boronic acid groups ($\text{B}(\text{OH})_2$) are fully polymerized.

At 550 K, we expect the hydroxyl groups to have desorbed as water, creating a fully deprotonated bidentate-bonded species, identical to that formed by the adsorption and ring opening of 2,4,6-triphenylboroxine. The only difference should be the additional upward-pointing and partially polymerized boronic acid group of 1,4-phenylenediboronic acid. As expected, we can nicely describe the spectrum at 550 K in Figure 8 with three peaks, representing intact upward-pointing boronic acid ($\text{B}-\text{OH}$) at 532.15 eV, upward-pointing boronic anhydride ($\text{B}-\text{O}-\text{B}$) at 532.03 eV, and the two $\text{Ti}-\text{O}-\text{B}$ bonds of the fully deprotonated bidentate-bonded species at 531.07 eV.

The $\text{Ti}-\text{O}-\text{B}$ peak is identical in shape (peak width and Gaussian-to-Lorentzian ratio) and position to that of adsorbed 2,4,6-triphenylboroxine, and, given the challenges involved with accurately subtracting the substrate contribution from the O 1s signal in Figure 6, we see that the peak area of this low-binding-energy peak for 1,4-phenylenediboronic acid (1220) and 2,4,6-triphenylboroxine (770) in Figure 8 scales well with the coverage ratio of 0.6:0.4.

As mentioned above, we can use the decreasing oxygen-to-boron ratio from Figure 8 to estimate a polymerization degree of 71% at 550 K. This means that out of 100 boronic acid ($\text{B}-\text{OH}$) groups, 71 will have polymerized, creating 35.5 boronic anhydride ($\text{B}-\text{O}-\text{B}$) groups. We therefore force the peaks at 532.15 and 532.03 eV, representing intact upward-pointing boronic acid ($\text{B}-\text{OH}$) and upward-pointing boronic anhydride ($\text{B}-\text{O}-\text{B}$), to have a peak ratio of 29:35.5, consistent with the polymerization degree of 71%. The boronic anhydride ($\text{B}-\text{O}-\text{B}$) peak is forced to have the same shape as the $\text{Ti}-\text{O}-\text{B}$ peak, but the intact boronic acid ($\text{B}-\text{OH}$) peak is forced to the same wider shape as in the 1.4 ML spectra, where the shape is easier to determine (see Figure 8).

The position of the boronic anhydride ($\text{B}-\text{O}-\text{B}$) peak at 532.03 eV is close to the positions of both the multilayers of 2,4,6-triphenylboroxine and the remaining layers after annealing multilayers of 1,4-phenylenediboronic acid at 600 K, which are both found at 532.2 eV in Figure 9. The position of the intact upward-pointing boronic acid ($\text{B}-\text{OH}$) at 532.15

eV in Figure 9 is shifted to lower binding energies compared to the multilayers of 1,4-phenylenediboronic acid at 532.9 eV. This could be due to differences in the hydrogen-bonding environment between multilayers of intact acid compared to upright-standing acid groups at the surface surrounded by anhydride groups. In general, we observe that we have to allow the intact acid peak to shift between the different species on the surface (see Figure 8).

We have argued that the density of the saturated monolayer strongly suggests that the monodentate adsorption mode dominates at 300 K. However, a bidentate adsorption mode could dominate at lower coverage. If we had a bidentate-bonded species at 300 K, we would expect two $\text{Ti}-\text{O}-\text{B}$ groups to remain on the surface after heating and two $\text{Ti}-\text{OH}$ groups to disappear. This behavior would only be consistent with our spectra if the $\text{Ti}-\text{OH}$ groups had to have an O 1s binding energy of about 531.94 eV (see Figure S9). This would be unusually high for hydroxyl groups on rutile $\text{TiO}_2(110)$, which typically have binding energies of 531.1–531.6 eV.^{23,32,33,55}

If instead we had a monodentate-bonded species at 300 K, we would expect one $\text{Ti}-\text{O}-\text{B}$ group, which would remain on the surface after heating, one $\text{B}-\text{OH}$ group, which would convert into a $\text{Ti}-\text{O}-\text{B}$ group upon heating, and one $\text{Ti}-\text{OH}$ group, which would disappear. This would be consistent with our spectra if the $\text{Ti}-\text{OH}$ group has an O 1s binding energy of 531.16 eV (see Figure S9), which is where one would expect to find surface hydroxyl groups on rutile $\text{TiO}_2(110)$. This is therefore the fit we have included in Figure 8.

The fit in Figure 8 also introduces a $\text{B}-\text{OH}$ group at the surface with a binding energy of 532.18 eV. We did not determine the position of this species from this fit, because of the overlap with the $\text{B}-\text{OH}$ groups pointing to the vacuum interface. Instead, we determined the position from the spectrum of 1.0 ML 4-acetylphenylboronic acid (discussed in detail below), which has no $\text{B}-\text{OH}$ groups at the vacuum interface.

In conclusion, 0.6 ML of 1,4-phenylenediboronic acid adsorbs at 300 K in a singly deprotonated monodentate configuration with an intact boronic-acid group pointing up away from the surface. At 550 K, the protons have desorbed as water, and the monodentate species has converted to a fully deprotonated bidentate species. In addition, most of the upward-pointing boronic-acid groups have polymerized.

1.3 ML 1,4-Phenylenediboronic Acid. The behavior of the O 1s and B 1s spectra of 1.3 ML 1,4-phenylenediboronic acid in the 300–550 K temperature range shows many similarities to the lower coverage, as is evident from Figures 2 and 7. The O 1s spectra have a prominent peak at 533 eV, that slightly decreases in intensity and shifts to lower binding energies upon heating, while the B 1s spectra remain unchanged. This behavior suggests that we have the same polymerization of the upward-pointing acid groups at the vacuum interface that we see at low coverage, but to a lesser extent. Based on the oxygen:boron ratio in Figure 8, we estimate a degree of polymerization of 31% at 550 K, corresponding to a boronic acid ($\text{B}-\text{OH}$) to boronic anhydride ($\text{B}-\text{O}-\text{B}$) ratio of 69:15.5. The higher degree of polymerization at lower coverages could be a result of a higher degree of flexibility in the adsorption structure at lower coverage, allowing the upward-pointing boronic acid groups at the vacuum interface to adopt a configuration more susceptible to anhydride formation.

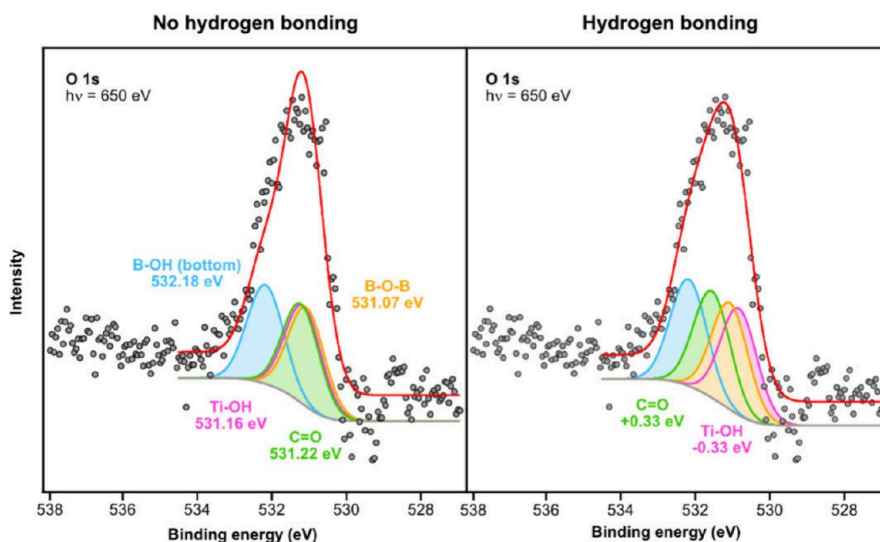


Figure 10. Hydrogen bonding within the 0.3 ML of 4-acetylphenylboronic acid layer at 300 K. Shifting the carbonyl (C=O) peak to higher binding energies and the surface hydroxyl (Ti–OH) peak to lower binding energies, consistent with hydrogen bonding between the two groups, significantly improves the quality of the fit.

At 300 K, we therefore assign the main O 1s peak at 532.41 eV to the upward-pointing acid groups at the vacuum interface. Using the peak shapes and positions from the 0.4 ML 2,4,6-triphenylboroxine and 0.6 ML 1,4-phenylenediboric acid spectra (B–OH (bottom) at 532.18 eV, Ti–O–B at 531.07 eV and Ti–OH at 531.16 eV), we can describe the small low-binding-energy shoulder at 531 eV as the same singly deprotonated monodentate configuration we observed for 0.6 ML. The 68% decrease in intensity of these peaks in Figure 8, from 710 at 0.6 ML to 230 at 1.3 ML, roughly scales with the 65% increased attenuation of the Ti 2p core level (not shown) caused by the increased thickness of the molecular layer. At 550 K, the small low-binding energy shoulder remains mostly unchanged, but this is consistent with our observations at 0.6 ML, where one B–OH group converts into a Ti–O–B group and one Ti–OH group is lost through desorption of water.

In conclusion, upon heating to 550 K, the degree of polymerization of the upward-pointing acid groups at the vacuum interface is lower at a coverage of 1.3 ML compared to 0.6 ML. The functional groups directly at the surface are strongly attenuated at 1.3 ML, but can be described by the same binding modes that we observed at 0.6 ML.

1.0 ML 4-Acetylphenylboronic Acid. For 4-acetylphenylboronic acid, the carbonyl (C=O) group is lost between 500–550 K, as can be seen in Figure 5, which is most likely a decomposition analogous to that of acetophenone, where the molecule decomposes into carbon monoxide and toluene.⁵⁶ For acetophenone, this decomposition occurs at 900 K, significantly higher than the 500–550 K observed here, but the boronic acid group as well as the presence of the surface could significantly lower the activation energy barrier.

The loss of the carbonyl group at 500–550 K overlaps with the desorption of protons as water and the appearance of the oxidized boron species at 550–600 K in Figure 2. This behavior makes any identification of the adsorbed species in this temperature range very difficult, so we will focus only on the adsorbed species at 300 K.

If 4-acetylphenylboronic acid adsorbs in the same singly deprotonated monodentate configuration as 1,4-phenylenediboric acid, we should be able to describe our measured O 1s

spectra with three components located close to the rutile TiO₂(110) surface (B–OH, Ti–O–B, and Ti–OH) and a fourth component potentially pointing into the vacuum (C=O). The carbonyl group (C=O) could therefore appear more intense in the O 1s spectrum than the other three groups because it is not attenuated by the phenyl ring of the molecule.

Indeed, if we look at the O 1s spectrum of 1.0 ML of 4-acetylphenylboronic acid at 300–450 K in Figure 8, it is nicely described by three peaks in a 1:1:1 ratio at the expected positions of boronic acid (B–OH) at 532.18 eV, Ti–O–B at 531.07 eV, and surface hydroxyl groups (Ti–OH) at 531.16 eV, in addition to a fourth more intense peak at 531.22 eV, which we assign to the upward-pointing carbonyl groups (C=O). The O 1s peak position of the carbonyl group of multilayers of pure 4-acetylphenylboronic acid is at 531.8 eV (see Figure 9). This peak position is significantly higher than what we observe for the monolayer, but it might change due to hydrogen bonding. For phthalic acid, for example, the splitting in the O 1s region between the hydroxyl (C–OH) and carbonyl (C=O) oxygen atoms of the carboxylic acid group decreases from 1.9 eV in the gas phase⁵⁷ to 1.1 eV in the condensed phase,⁵⁸ because the hydroxyl (C–OH) groups form hydrogen bonds to the carbonyl (C=O) groups. The same trend is observed for gas phase and multilayer spectra of formic acid^{59,60} or acrylic acid.^{60,61} This means that we can expect hydrogen bonding to shift hydroxyl groups to lower binding energies and carbonyl groups to higher binding energies. We therefore assign the lower binding energy of 531.22 eV observed for the carbonyl group in the monolayer, compared to the multilayer, to an absence of hydrogen bonding in the upward-pointing carbonyl groups of the saturated monolayer.

0.3 ML 4-Acetylphenylboronic Acid. At a coverage of 0.3 ML, the O 1s spectra of 4-acetylphenylboronic acid in Figure 7a look quite different from the spectra of the full monolayer, that is, the intense peak of the carbonyl group (C=O) at 531.22 eV is missing. This observation suggests a change in orientation of the molecule, moving the carbonyl group closer to the surface, and thereby causing the attenuation of the carbonyl group to become similar to that

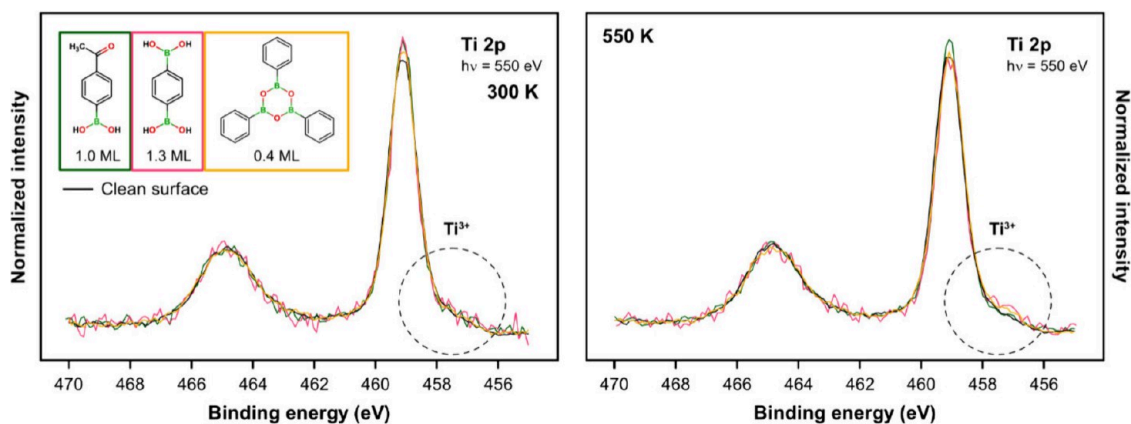


Figure 11. Ti 2p region of the three boronic acid derivatives on rutile $\text{TiO}_2(110)$ at 300 K (left) and 550 K (right) after normalization and linear-background subtraction. The Ti^{3+} shoulder does not change upon adsorption of the molecules at 300 K, indicating that the number of small polarons in the surface-near region is not affected by the adsorption of the molecules. At 550 K, the Ti^{3+} shoulder does not change for 4-acetylphenylboronic acid, but it slightly increases for 2,4,6-triphenylboroxine and 1,4-phenylenediboronic acid.

of the other three functional groups (B–OH, Ti–O–B, and Ti–OH). This orientation is consistent with our C K-edge NEXAFS spectra in Figure 4, which indicate that the phenyl ring polar angle decreases from 68° at 1.0 ML to 37° at 0.3 ML, thus becoming more flat lying. A driving force for this reorientation could be hydrogen bonding between the carbonyl groups and either the boronic acid groups (B–OH) of a neighboring molecule or the surface hydroxyl groups (Ti–OH). This conclusion is supported by the C 1s spectra in Figure 5, where the different binding energy position of the carbonyl signal clearly indicates a different chemical environment of the carbonyl group at low coverage.

As can be seen in Figure 10, the O 1s spectrum of 0.3 ML of 4-acetylphenylboronic acid is described reasonably well by four peaks in a 1:1:1:1 ratio at the same binding energy positions as for the full monolayer, consistent with identical attenuation of the carbonyl group and the other three functional groups. However, the fit improves significantly if the binding energy position of the carbonyl group in Figure 10 is allowed to increase from 531.22 to 531.55 eV and the binding energy position of the surface hydroxyl groups (Ti–OH) is allowed to decrease from 531.16 to 530.83 eV. As discussed above for the multilayer and gas-phase spectra of carboxylic acids, the magnitude and direction of these shifts are entirely consistent with what would be expected if hydrogen bonds were formed between the surface hydroxyl groups (Ti–OH) and the carbonyl groups (C = O) of the molecule.

Because of the uncertainties of the substrate peak subtraction, we are not confident to conclude hydrogen bonding based on the O 1s fits alone. However, the position of the carbonyl group in the C 1s region and the phenyl ring orientation in C K-edge NEXAFS both suggests hydrogen bonding. In addition, the change in orientation is also visible in the C 1s region in Figure S10, where the apparent ratio of phenyl (C_{ph}) and methyl ($-\text{CH}_3$) carbon to carbonyl (C=O) carbon changes from 7.4 to 10.3 as the coverage is decreased from 1.0 to 0.3 ML, consistent with the carbonyl group being attenuated by the phenyl ring at low coverage. The nominal ratio of phenyl and methyl carbon to carbonyl carbon in 4-acetylphenylboronic acid is 7, but the observed ratio can be affected by factors such as photoelectron diffraction and orientation of the molecule. The attenuation of the carbonyl group becomes even more apparent when comparing the peak-

area ratio of carbonyl carbon to boron in Figure 8 and Figure S10, which decreases by 40% as the coverage is decreased from 1.0 to 0.3 ML. We would therefore expect an identical decrease in the carbonyl oxygen:boron ratio. Indeed, if we compare the carbonyl oxygen:boron peak-area ratio obtained from our fits in Figure 8, we find a 51% decrease, which is a very reasonable agreement. We are only able to make these direct comparisons, because we measure all core levels with very similar kinetic energies (90–120 eV) of the emitted photoelectrons.

In conclusion, 4-acetylphenylboronic acid adsorbs at 300 K in the same singly deprotonated monodentate configuration as 1,4-phenylenediboronic acid. In the full monolayer, the carbonyl groups point away from the surface, but at low coverage, they bend down toward the surface, most likely forming hydrogen bonds with hydroxyl groups on the surface.

Much of the above analysis is based on fitting the O 1s core levels after subtraction of the substrate contribution. However, when analyzing these data, it is always important to keep the uncertainties introduced by the subtraction of the substrate in mind, which particularly affect the low-binding energy shoulders, since small errors in the substrate peak position will cause significant changes in the low-binding energy shoulder. This, in turn, can make peaks appear to be more asymmetric than they actually are. For 2,4,6-triphenylboroxine, for example, the fit to the experimental data averaged from 300–550 K could be improved by adding a B–O–B species at 532.03 eV to the asymmetric signal after substrate subtraction. A second species would indicate an incomplete ring-opening reaction, but given the uncertainty of the substrate subtraction, we simply cannot make any reliable statements about such minority species. In general, we are unable to identify any minority species on the surface, for example, boronic acid dimers formed by B–O–B bond formation between neighboring boronic acid groups.⁴¹

Polarons. Rutile TiO_2 is known to form small polarons when the crystal is reduced.^{62–65} Such reduction can occur through surface or bulk oxygen vacancies, titanium interstitials or impurities within the crystal. This effectively injects an excess electron into the crystal, which locally distorts the crystal lattice around a single titanium atom, reducing the titanium atom from Ti^{4+} to Ti^{3+} and creating a new band gap state with Ti 3d¹ character and a Ti^{3+} shoulder in the Ti 2p core-level region. For the rutile $\text{TiO}_2(110)$ surface, these small

polarons are concentrated in the second layer below the surface and can strongly interact with and affect the adsorption of molecules, such as oxygen,⁶⁶ carbon monoxide,^{67,68} NO,⁶⁸ water,^{69,70} and formic,⁷¹ acetic,⁷¹ and phosphonic²³ acids.

The Ti 3d¹ bandgap state at 1 eV is clearly visible in our valence-band spectra in Figure S8. Unfortunately, the photon beam at the low photon energy of the valence-band measurements (43 eV) became broader than we expected, causing the beam to extend over the edge of the crystal at some positions, thereby resulting in a loss of total intensity. We have corrected for this by normalizing all valence band spectra to their total integrated area. This means that we can compare the spectra qualitatively, but we are reluctant to draw conclusions based on quantitative changes in peak areas, such as the Ti 3d¹ bandgap state.

Fortunately, the Ti 2p spectra in Figure 11 are unaffected by this, and there the Ti³⁺ low-binding-energy shoulder remains unchanged upon adsorption of our three boronic acid derivatives at room temperature. This is in contrast to formic,⁷¹ acetic,⁷¹ and phosphonic²³ acids, which have been shown to strongly affect the concentration of small polarons in the near-surface region. An important factor could be the pronounced relaxation of the near-surface region of the rutile TiO₂(110) substrate upon adsorption of the molecules. Since polarons induce local lattice distortions,^{63,72} the stabilities of polarons will be affected by lattice distortions. The strong relaxation of the clean rutile TiO₂(110) surface is one of the factors stabilizing small polarons in the second layer,^{72–74} and the re-relaxation of the lattice back to its bulk positions could explain the disappearance of small polarons from the near-surface region, as suggested by the data for the adsorption of phenylphosphonic acid.²³ This re-relaxation of the lattice back to the original bulk parameters is also visible in the O 1s region as a narrowing of the substrate O 1s contribution.²³ The fact that we do not see the same narrowing of the substrate contribution in the O 1s region is an indication that we do not have the same re-relaxation of the surface as observed for phenylphosphonic acid. This could be one explanation for why the concentration of polarons we observe in the near-surface region remains unchanged upon adsorption of our three boronic acid derivatives at room temperature.

We observe a change in the adsorption binding mode from monodentate to bidentate upon desorption of surface OH groups. For phenylphosphonic acid, the high-temperature adsorption mode massively increased the Ti³⁺ signal.²³ We observe that the Ti³⁺ shoulder of 4-acetylphenylboronic acid in Figure 11 does not change upon annealing to 550 K, but there is a slight increase in the Ti³⁺ signal for 2,4,6-triphenylboroxine and 1,4-phenylenediboronic acid. This indicates a slight increase in the surface-near polaron concentration, but this is significantly less pronounced than the changes observed for phenylphosphonic acid²³ and clearly indicates only a weak influence of phenylboronic acid derivatives on the surface-near polaron concentration.

In conclusion, the adsorption of our three boronic acid derivatives has no significant effect on the concentration of polarons in the near-surface region at room temperature and after annealing to 550 K.

B₂O₃ Formation above 550 K. Above 550 K a new oxidized boron species appears in the B 1s spectra in Figure 2 at 192.4 eV for all three boronic acid derivatives. This observation suggests boron with an additional bond to oxygen. However, if we were to form tetrahedrally coordinated boron

(with three oxygen and one carbon bond), we would lose the planar nature of the boron group and therefore the π^* resonances in B K-edge NEXAFS. However, we still observe a clear π^* resonance at 193.8 eV, indicating a planar trigonal rather than tetrahedral boron geometry,^{27,29} which is only possible if we break the carbon–boron bond when forming the additional bond to oxygen.

The B 1s, O 1s, and B π^* peak positions at 192.4, 531.3, and 193.7 eV are in decent agreement with the literature values for trigonal planar B₂O₃ of 192–194,^{28,75,76} 532.5–533.6,^{75–77} and 194 eV,^{27–29} respectively. We therefore suggest that the reaction at 600–700 K is a cleavage of the carbon–boron bond and the formation of boron oxide.

We do observe a gradual decrease in carbon coverage on the surface with increasing temperature in Figure 5, but for none of the three molecules do we observe an abrupt decrease in carbon coverage at 600–700 K. This observation suggests that after the carbon–boron bond cleavage carbon remains on the surface in some form, possibly as some sort of carbonaceous network.

CONCLUSIONS

We successfully deposited intact 4-acetylphenylboronic acid, 1,4-phenylenediboronic acid, and 2,4,6-triphenylboroxine on rutile TiO₂(110). We find that both 4-acetylphenylboronic acid and 1,4-phenylenediboronic acid adsorb in a singly deprotonated monodentate configuration at 300–400 K, while 2,4,6-triphenylboroxine undergoes a ring-opening reaction already at 300 K, forming a fully deprotonated bidentate-bonded species.

Based on the angular dependency in C K-edge NEXAFS and the attenuations of the B 1s, C 1s, and O 1s core levels, we find that 4-acetylphenylboronic acid to be relatively upright standing in the full monolayer, but more flat lying at lower coverage, and we suggest that the same is true for 1,4-phenylenediboronic acid. For 4-acetylphenylboronic acid, one of the driving forces for the change in orientation could be the formation of hydrogen bonds between the carbonyl group (C=O) of the molecule and hydroxyl groups (Ti–OH) on the surface at low coverage.

At elevated temperatures, above 500 K, protons desorb from the rutile TiO₂(110) surface as water, creating oxygen vacancies, and 1,4-phenylenediboronic acid converts from a monodentate to a fully deprotonated bidentate species. In addition, the upward-pointing boronic-acid groups polymerize into chains of boronic anhydride. For 4-acetylphenylboronic acid, we expect the same conversion from monodentate to fully deprotonated bidentate above 500 K, but the loss of the carbonyl (C=O) group between 500–550 K complicates the interpretation of the O 1s spectrum.

Above 550 K, the B 1s, O 1s, and B π^* peak positions suggest cleavage of the carbon–boron bond and the formation of trigonal planar B₂O₃.

In contrast to the adsorption of carboxylic⁷¹ and phosphonic acids,²³ we find that the concentration of surface-near small polarons, as observed in the Ti 2p region, is not affected by the adsorption of the three boronic acid derivatives.

ASSOCIATED CONTENT

Data Availability Statement

Data openly available in a public repository (<https://doi.org/10.5281/zenodo.11108104>).

SI Supporting Information

The Supporting Information is available free of charge at <https://pubs.acs.org/doi/10.1021/acs.jpcc.4c03264>.

Additional information on molecular integrity of the three boronic acid derivatives; details on NEXAFS angular dependency; photon flux for B and C K-edge NEXAFS; second-order light correction in C K-edge NEXAFS; details on DFT calculations, optimized structures, and predicted X-ray absorption spectra; coverage evolution as a function of temperature; valence-band spectra; calculation of the polymerization degree of 1,4-phenylenediboronic acid; comparison of a monodentate and bidentate fit model to experimental O 1s data; fits to selected C 1s core level spectra (PDF)

AUTHOR INFORMATION**Corresponding Author**

Ole Lytken – *Lehrstuhl für Physikalische Chemie 2, Friedrich-Alexander-Universität Erlangen-Nürnberg, Erlangen 91058, Germany*; orcid.org/0000-0003-0572-0827;
Email: ole.lytken@fau.de

Authors

Alexander Wolfram – *Lehrstuhl für Physikalische Chemie 2, Friedrich-Alexander-Universität Erlangen-Nürnberg, Erlangen 91058, Germany*; orcid.org/0000-0002-0883-7724

Maximilian Muth – *Lehrstuhl für Physikalische Chemie 2, Friedrich-Alexander-Universität Erlangen-Nürnberg, Erlangen 91058, Germany*; orcid.org/0000-0001-6937-8851

Federico J. Williams – *Departamento de Química Inorgánica, Analítica y Química Física, Facultad de Ciencias Exactas y Naturales, INQUIMAE-CONICET, Universidad de Buenos Aires, Buenos Aires C1428EHA, Argentina*; orcid.org/0000-0002-6194-2734

Sascha Mehl – *Eletra-Sincrotrone Trieste SCpA, Basovizza, Trieste 34149, Italy*; orcid.org/0000-0002-0228-177X

Nataliya Tsud – *Department of Surface and Plasma Science, Charles University, Faculty of Mathematics and Physics, Prague 18000, Czech Republic*; orcid.org/0000-0001-7439-7731

Hans-Peter Steinrück – *Lehrstuhl für Physikalische Chemie 2, Friedrich-Alexander-Universität Erlangen-Nürnberg, Erlangen 91058, Germany*; orcid.org/0000-0003-1347-8962

Complete contact information is available at:
<https://pubs.acs.org/doi/10.1021/acs.jpcc.4c03264>

Notes

The authors declare no competing financial interest.

ACKNOWLEDGMENTS

The authors acknowledge the CERIC–ERIC Consortium for the access to experimental facilities and financial support, we acknowledge financial support from CONICET (PIP2001), and thank the German Research Foundation (DFG) for financial funding through FOR 1878 (funCOS). The Ministry of Education, Youth and Sports of the Czech Republic is acknowledged for financial support under project LM2023072.

REFERENCES

- (1) Suzuki, A. Organoborane coupling reactions (Suzuki coupling). *Proc. Jpn. Acad., Ser. B: Phys. Biol. Sci.* **2004**, *80* (8), 359–371.
- (2) Lennox, A. J.; Lloyd-Jones, G. C. Selection of boron reagents for Suzuki–Miyaura coupling. *Chem. Soc. Rev.* **2014**, *43* (1), 412–443.
- (3) Hooshmand, S. E.; Heidari, B.; Sedghi, R.; Varma, R. S. Recent advances in the Suzuki–Miyaura cross-coupling reaction using efficient catalysts in eco-friendly media. *Green Chem.* **2019**, *21* (3), 381–405.
- (4) Jäkle, F. Borylated Polyolefins and their Applications. *J. Inorg. Organomet. Polym. Mater.* **2005**, *15* (3), 293–307.
- (5) Cui, Y.; Chen, F.; Yin, X.-B. A ratiometric fluorescence platform based on boric-acid-functional Eu-MOF for sensitive detection of H₂O₂ and glucose. *Biosens. Bioelectron.* **2019**, *135*, 208–215.
- (6) Cao, Q.; Peng, Y.; Yu, Q.; Shi, Z.; Jia, Q. Post synthetic modification of Zr-MOF with phenylboronic acid: Fluorescence sensing of sialic acid. *Dyes Pigm.* **2022**, *197*, No. 109839.
- (7) Zhu, X.; Gu, J.; Zhu, J.; Li, Y.; Zhao, L.; Shi, J. Metal–Organic Frameworks with Boronic Acid Suspended and Their Implication for cis-Diol Moieties Binding. *Adv. Funct. Mater.* **2015**, *25* (25), 3847–3854.
- (8) Pappin, B.; Kiefel, M. J.; Houston, T. A. Boron–Carbohydrate Interactions. In *Carbohydrates—Comprehensive Studies on Glycobiology and Glycotechnology*; Chuan-Fa, C., Ed.; IntechOpen: Rijeka, Croatia, 2012; pp 37–54.
- (9) Wang, X.; Xia, N.; Liu, L. Boronic Acid-Based Approach for Separation and Immobilization of Glycoproteins and Its Application in Sensing. *Int. J. Mol. Sci.* **2013**, *14* (10), 20890–20912.
- (10) Vericat, C.; Vela, M.; Benitez, G.; Carro, P.; Salvarezza, R. Self-assembled monolayers of thiols and dithiols on gold: new challenges for a well-known system. *Chem. Soc. Rev.* **2010**, *39* (5), 1805–1834.
- (11) Love, J. C.; Estroff, L. A.; Kriebel, J. K.; Nuzzo, R. G.; Whitesides, G. M. Self-assembled monolayers of thiolates on metals as a form of nanotechnology. *Chem. Rev.* **2005**, *105* (4), 1103–1170.
- (12) Ahangaran, F.; Navarchian, A. H. Recent advances in chemical surface modification of metal oxide nanoparticles with silane coupling agents: A review. *Adv. Colloid Interface Sci.* **2020**, *286*, No. 102298.
- (13) Wang, L.; Schubert, U. S.; Hoepfner, S. Surface chemical reactions on self-assembled silane based monolayers. *Chem. Soc. Rev.* **2021**, *50* (11), 6507–6540.
- (14) Zhang, L.; Cole, J. M. Anchoring groups for dye-sensitized solar cells. *ACS Appl. Mater. Interfaces* **2015**, *7* (6), 3427–3455.
- (15) Pujari, S. P.; Scheres, L.; Marcelis, A. T. M.; Zuillhof, H. Covalent Surface Modification of Oxide Surfaces. *Angew. Chem., Int. Ed.* **2014**, *53* (25), 6322–6356.
- (16) Demadis, K. D.; Papadaki, M.; Raptis, R. G.; Zhao, H. Corrugated, Sheet-Like Architectures in Layered Alkaline-Earth Metal R₂S-Hydroxyphosphonoacetate Frameworks: Applications for Anti-corrosion Protection of Metal Surfaces. *Chem. Mater.* **2008**, *20* (15), 4835–4846.
- (17) Boissezon, R.; Muller, J.; Beaugeard, V.; Monge, S.; Robin, J.-J. Organophosphonates as anchoring agents onto metal oxide-based materials: synthesis and applications. *RSC Adv.* **2014**, *4* (67), 35690–35707.
- (18) Akin Kara, D.; Kara, K.; Oylumluoglu, G.; Yigit, M. Z.; Can, M.; Kim, J. J.; Burnett, E. K.; Gonzalez Arellano, D. L.; Buyukcelebi, S.; Ozel, F.; et al. Enhanced Device Efficiency and Long-Term Stability via Boronic Acid-Based Self-Assembled Monolayer Modification of Indium Tin Oxide in a Planar Perovskite Solar Cell. *ACS Appl. Mater. Interfaces* **2018**, *10* (35), 30000–30007.
- (19) Kirbiyik, Ç.; Akin Kara, D.; Kara, K.; Buyukcelebi, S.; Yigit, M. Z.; Can, M.; Kus, M. Improving the performance of inverted polymer solar cells through modification of compact TiO₂ layer by different boronic acid functionalized self-assembled monolayers. *Appl. Surf. Sci.* **2019**, *479*, 177–184.
- (20) Schlögl, S.; Sirtl, T.; Eichhorn, J.; Heckl, W. M.; Lackinger, M. Synthesis of two-dimensional phenylene–boroxine networks through in vacuo condensation and on-surface radical addition. *Chem. Commun.* **2011**, *47* (45), 12355–12357.

- (21) Ourdjini, O.; Pawlak, R.; Abel, M.; Clair, S.; Chen, L.; Bergeon, N.; Sassi, M.; Oison, V.; Debieer, J.-M.; Coratger, R.; Porte, L. Substrate-mediated ordering and defect analysis of a surface covalent organic framework. *Phys. Rev. B* **2011**, *84* (12), No. 125421.
- (22) Leiding, P.; Panighel, M.; Perez Dieste, V.; Villar-Garcia, I. J.; Vezzoni, P.; Haag, F.; Barth, J. V.; Allegretti, F.; Gunther, S.; Patera, L. L. Probing dynamic covalent chemistry in a 2D boroxine framework by in situ near-ambient pressure X-ray photoelectron spectroscopy. *Nanoscale* **2023**, *15* (3), 1068–1075.
- (23) Wolfram, A.; Muth, M.; Köbl, J.; Mölkner, A.; Tsud, N.; Mehl, S.; Steinrück, H.-P.; Meyer, B.; Lytken, O., Phenylphosphonic acid on rutile TiO₂(110): Using theoretically predicted O 1s spectra to identify the adsorption binding modes. *J. Phys. Chem. C* **2024**. DOI: 10.1021/acs.jpcc.4c03690
- (24) Rangan, S.; Ruggieri, C.; Bartynski, R.; Martínez, J. I.; Flores, F.; Ortega, J. Densely Packed ZnTPPs Monolayer on the Rutile TiO₂(110)-(1 × 1) Surface: Adsorption Behavior and Energy Level Alignment. *J. Phys. Chem. C* **2016**, *120* (8), 4430–4437.
- (25) Materials Science Beamline. Available at: <https://www.elettra.eu/lightsources/elettra/elettra-beamlines/msb/specifications.html> (accessed Jan. 19, 2024).
- (26) Lytken, O.; Wechsler, D.; Steinrück, H.-P. Removing photoemission features from Auger-yield NEXAFS spectra. *J. Electron Spectrosc. Relat. Phenom.* **2017**, *218*, 35–39.
- (27) Xu, D.; Peak, D. Adsorption of Boric Acid on Pure and Humic Acid Coated am-Al(OH)₃: A Boron K-Edge XANES Study. *Environ. Sci. Technol.* **2007**, *41* (3), 903–908.
- (28) Zhang, Z.; Yamaguchi, E. S.; Kasrai, M.; Bancroft, G. M. Interaction of ZDDP with Borated Dispersant Using XANES and XPS. *Tribol. Trans.* **2004**, *47* (4), 527–536.
- (29) Duffin, A. M.; Schwartz, C. P.; England, A. H.; Uejio, J. S.; Prendergast, D.; Saykally, R. J. pH-dependent x-ray absorption spectra of aqueous boron oxides. *J. Chem. Phys.* **2011**, *134* (15), No. 154503.
- (30) Thomas, A. G.; Syres, K. L. Adsorption of organic molecules on rutile TiO₂ and anatase TiO₂ single crystal surfaces. *Chem. Soc. Rev.* **2012**, *41* (11), 4207–4217.
- (31) Pang, C. L.; Lindsay, R.; Thornton, G. Structure of Clean and Adsorbate-Covered Single-Crystal Rutile TiO₂ Surfaces. *Chem. Rev.* **2013**, *113* (6), 3887–3948.
- (32) Fernández, C. C.; Wechsler, D.; Rocha, T. C.; Steinrück, H.-P.; Lytken, O.; Williams, F. J. Adsorption of phosphonic-acid-functionalized porphyrin molecules on TiO₂(110). *J. Phys. Chem. C* **2019**, *123* (17), 10974–10980.
- (33) Köbl, J.; Wechsler, D.; Kataev, E. Y.; Williams, F. J.; Tsud, N.; Franchi, S.; Steinrück, H.-P.; Lytken, O. Adsorption of phenylphosphonic acid on rutile TiO₂(110). *Surf. Sci.* **2020**, *698*, 121612.
- (34) Li, S.-C.; Wang, J.-g.; Jacobson, P.; Gong, X. Q.; Selloni, A.; Diebold, U. Correlation between Bonding Geometry and Band Gap States at Organic–Inorganic Interfaces: Catechol on Rutile TiO₂(110). *J. Am. Chem. Soc.* **2009**, *131* (3), 980–984.
- (35) O'Rourke, C.; Bowler, D. R. DSSC anchoring groups: a surface dependent decision. *J. Phys.: Condens. Matter* **2014**, *26* (19), 195302.
- (36) Kurtz, R. L.; Stock-Bauer, R.; Msdey, T. E.; Román, E.; De Segovia, J. Synchrotron radiation studies of H₂O adsorption on TiO₂(110). *Surf. Sci.* **1989**, *218* (1), 178–200.
- (37) Krischok, S.; Höfft, O.; Günster, J.; Stultz, J.; Goodman, D. W.; Kemper, V. H₂O interaction with bare and Li-precovered TiO₂: studies with electron spectroscopies (MIES and UPS(HeI and II)). *Surf. Sci.* **2001**, *495* (1), 8–18.
- (38) Hugenschmidt, M. B.; Gamble, L.; Campbell, C. T. The interaction of H₂O with a TiO₂(110) surface. *Surf. Sci.* **1994**, *302* (3), 329–340.
- (39) Petrik, N. G.; Kimmel, G. A. Reaction kinetics of water molecules with oxygen vacancies on rutile TiO₂(110). *J. Phys. Chem. C* **2015**, *119* (40), 23059–23067.
- (40) Aizawa, M.; Morikawa, Y.; Namai, Y.; Morikawa, H.; Iwasawa, Y. Oxygen vacancy promoting catalytic dehydration of formic acid on TiO₂(110) by in situ scanning tunneling microscopic observation. *J. Phys. Chem. B* **2005**, *109* (40), 18831–18838.
- (41) Raghunath, P.; Lin, M. C. Adsorption Configurations and Decomposition Pathways of Boric Acid on TiO₂ Rutile (110) Surface: A Computational Study. *J. Phys. Chem. C* **2009**, *113* (9), 3751–3762.
- (42) Chung, D. Review graphite. *J. Mater. Sci.* **2002**, *37*, 1475–1489.
- (43) Rheingold, A. L.; Moore, C. E. CCDC 915342: *Experimental Crystal Structure Determination*; Cambridge Crystallographic Data Centre, 2013.
- (44) Bolte, M. CCDC 243438: *Experimental Crystal Structure Determination*; Cambridge Crystallographic Data Centre, 2005.
- (45) Tojo, K.; Mizuguchi, J. Refinement of the crystal structure of α -3,4,9,10-perylenetetracarboxylic dianhydride, C₂₄H₈O₆, at 223 K. *Z. Kristallogr. N. Cryst.* **2002**, *217* (JG), 253–254.
- (46) Tojo, K.; Mizuguchi, J. Refinement of the crystal structure of β -3,4,9,10-perylenetetracarboxylic dianhydride, C₂₄H₈O₆, at 223 K. *Z. Kristallogr. N. Cryst.* **2002**, *217* (JG), 255–256.
- (47) Katrusiak, A.; Podsiadlo, M.; Budzianowski, A. Association CH $\cdots\pi$ and No van der Waals Contacts at the Lowest Limits of Crystalline Benzene I and II Stability Regions. *Cryst. Growth Des.* **2010**, *10* (8), 3461–3465.
- (48) Schwarz, M.; Hohner, C.; Mohr, S.; Libuda, J. Dissociative Adsorption of Benzoic Acid on Well-Ordered Cobalt Oxide Surfaces: Role of the Protons. *J. Phys. Chem. C* **2017**, *121* (51), 28317–28327.
- (49) Rahe, P.; Nimmrich, M.; Nefedov, A.; Naboka, M.; Wöll, C.; Kuhnle, A. Transition of molecule orientation during adsorption of terephthalic acid on rutile TiO₂(110). *J. Phys. Chem. C* **2009**, *113* (40), 17471–17478.
- (50) Du, Y.; Petrik, N. G.; Deskins, N. A.; Wang, Z.; Henderson, M. A.; Kimmel, G. A.; Lyubintsev, I. Hydrogen reactivity on highly-hydroxylated TiO₂(110) surfaces prepared via carboxylic acid adsorption and photolysis. *Phys. Chem. Chem. Phys.* **2012**, *14* (9), 3066–3074.
- (51) White, J. M.; Szanyi, J.; Henderson, M. A. The Photon-Driven Hydrophilicity of Titania: A Model Study Using TiO₂(110) and Adsorbed Trimethyl Acetate. *J. Phys. Chem. B* **2003**, *107* (34), 9029–9033.
- (52) Lindsay, R.; Tomic, S.; Wander, A.; García-Méndez, M.; Thornton, G. Low Energy Electron Diffraction Study of TiO₂(110)(2 × 1)-[HCOO]⁻. *J. Phys. Chem. C* **2008**, *112* (36), 14154–14157.
- (53) Sayago, D. I.; Polcik, M.; Lindsay, R.; Toomes, R. L.; Hoeft, J. T.; Kittel, M.; Woodruff, D. P. Structure Determination of Formic Acid Reaction Products on TiO₂(110). *J. Phys. Chem. B* **2004**, *108* (38), 14316–14323.
- (54) Hall, D. G. Structure, Properties, and Preparation of Boronic Acid Derivatives. *In Boronic Acids* **2011**, 1–133.
- (55) Zhang, W.; Cao, L.; Wan, L.; Liu, L.; Xu, F. A Photoelectron Spectroscopy Study on the Interfacial Chemistry and Electronic Structure of Terephthalic Acid Adsorption on TiO₂(110)-(1 × 1) Surface. *J. Phys. Chem. C* **2013**, *117* (41), 21351–21358.
- (56) Smith, R.; Hinshelwood, C. N. The kinetics of the thermal decomposition of acetophenone. *Proc. R. Soc. A* **1940**, *176* (967), 468–473.
- (57) McQuaide, B.; Banna, M. The core binding energies of some gaseous aromatic carboxylic acids and their relationship to proton affinities and gas phase acidities. *Can. J. Chem.* **1988**, *66* (8), 1919–1922.
- (58) Kataev, E. Y.; Fromm, L.; Tariq, Q.; Wechsler, D.; Williams, F. J.; Tsud, N.; Franchi, S.; Steinrück, H.-P.; Görling, A.; Lytken, O. Anchoring of phthalic acid on MgO(100). *Surf. Sci.* **2022**, *720*, 122007.
- (59) Au, C. T.; Hirsch, W.; Hirschwald, W. Adsorption and interaction of carbon dioxide, formic acid and hydrogen/carbon dioxide mixtures on (1010) zinc oxide surfaces studied by photoelectron spectroscopy (XPS and UPS). *Surf. Sci.* **1988**, *199* (3), 507–517.
- (60) Naves de Brito, A.; Keane, M. P.; Correia, N.; Svensson, S.; Gelius, U.; Lindberg, B. J. Experimental and theoretical XPS study of model molecules for poly(methyl methacrylate). *Surf. Interface Anal.* **1991**, *17* (2), 94–104.

- (61) Bournel, F.; Laffon, C.; Parent, P.; Tourillon, G. Adsorption of some substituted ethylene molecules on Pt(111) at 95 K Part 1: NEXAFS. *XPS and UPS studies. Surf. Sci.* **1996**, *350* (1–3), 60–78.
- (62) Yin, W.-J.; Wen, B.; Zhou, C.; Selloni, A.; Liu, L.-M. Excess electrons in reduced rutile and anatase TiO₂. *Surf. Sci. Rep.* **2018**, *73* (2), 58–82.
- (63) Setvin, M.; Franchini, C.; Hao, X.; Schmid, M.; Janotti, A.; Kaltak, M.; Van de Walle, C. G.; Kresse, G.; Diebold, U. Direct View at Excess Electrons in TiO₂ Rutile and Anatase. *Phys. Rev. Lett.* **2014**, *113* (8), No. 086402.
- (64) Li, M.; Hebenstreit, W.; Diebold, U.; Tyryshkin, A. M.; Bowman, M. K.; Dunham, G. G.; Henderson, M. A. The Influence of the Bulk Reduction State on the Surface Structure and Morphology of Rutile TiO₂(110) Single Crystals. *J. Phys. Chem. B* **2000**, *104* (20), 4944–4950.
- (65) Livraghi, S.; Rolando, M.; Maurelli, S.; Chiesa, M.; Paganini, M. C.; Giamello, E. Nature of Reduced States in Titanium Dioxide as Monitored by Electron Paramagnetic Resonance. II: Rutile and Brookite Cases. *J. Phys. Chem. C* **2014**, *118* (38), 22141–22148.
- (66) Sokolović, I.; Reticcioli, M.; Čalkovský, M.; Wagner, M.; Schmid, M.; Franchini, C.; Diebold, U.; Setvin, M. Resolving the adsorption of molecular O₂ on the rutile TiO₂(110) surface by noncontact atomic force microscopy. *Proc. Natl. Acad. Sci. U.S.A.* **2020**, *117* (26), 14827–14837.
- (67) Reticcioli, M.; Sokolović, I.; Schmid, M.; Diebold, U.; Setvin, M.; Franchini, C. Interplay between Adsorbates and Polarons: CO on Rutile TiO₂(110). *Phys. Rev. Lett.* **2019**, *122* (1), No. 016805.
- (68) Cao, Y.; Yu, M.; Qi, S.; Huang, S.; Wang, T.; Xu, M.; Hu, S.; Yan, S. Scenarios of polaron-involved molecular adsorption on reduced TiO₂(110) surfaces. *Sci. Rep.* **2017**, *7* (1), 6148.
- (69) Yim, C. M.; Chen, J.; Zhang, Y.; Shaw, B.-J.; Pang, C. L.; Grinter, D. C.; Bluhm, H.; Salmeron, M.; Muryu, C. A.; Michaelides, A.; Thornton, G. Visualization of water-induced surface segregation of polarons on rutile TiO₂(110). *J. Phys. Chem. Lett.* **2018**, *9* (17), 4865–4871.
- (70) Li, Y.-B.; Si, R.; Wen, B.; Wei, X.-L.; Seriani, N.; Yin, W.-J.; Gebauer, R. The Role of Water Molecules on Polaron Behavior at Rutile(110) Surface: A Constrained Density Functional Theory Study. *J. Phys. Chem. Lett.* **2024**, *15* (4), 1019–1027.
- (71) Tanner, A. J.; Wen, B.; Ontaneda, J.; Zhang, Y.; Grau-Crespo, R.; Fielding, H. H.; Selloni, A.; Thornton, G. Polaron-adsorbate coupling at the TiO₂(110)-carboxylate interface. *J. Phys. Chem. Lett.* **2021**, *12* (14), 3571–3576.
- (72) Deskins, N. A.; Rousseau, R.; Dupuis, M. Distribution of Ti³⁺ Surface Sites in Reduced TiO₂. *J. Phys. Chem. C* **2011**, *115* (15), 7562–7572.
- (73) Reticcioli, M.; Setvin, M.; Schmid, M.; Diebold, U.; Franchini, C. Formation and dynamics of small polarons on the rutile TiO₂(110) surface. *Phys. Rev. B* **2018**, *98* (4), No. 045306.
- (74) Shibuya, T.; Yasuoka, K.; Mirbt, S.; Sanyal, B. A systematic study of polarons due to oxygen vacancy formation at the rutile TiO₂(110) surface by GGA+U and HSE06 methods. *J. Phys.: Condens. Matter* **2012**, *24* (43), No. 435504.
- (75) Joyner, D. J.; Hercules, D. M. Chemical bonding and electronic structure of B₂O₃, H₃BO₃, and BN: An ESCA, Auger, SIMS, and SXS study. *J. Chem. Phys.* **1980**, *72* (2), 1095–1108.
- (76) Gouin, X.; Grange, P.; Bois, L.; L'Haridon, P.; Laurent, Y. Characterization of the nitridation process of boric acid. *J. Alloys Compd.* **1995**, *224* (1), 22–28.
- (77) Strohmeier, B. R. Surface characterization of aluminum foil annealed in the presence of ammonium fluoborate. *Appl. Surf. Sci.* **1989**, *40* (3), 249–263.